NTNU
Norwegian University of
Science and Technology

Stabilized Camera for a Nano-UAV

Sindre Kløw Kjenstad

Master of Science in Engineering Cybernetics
Submission date: June 2010
Supervisor: Jan Tommy Gravdahl, ITK

Norwegian University of Science and Technology
Department of Engineering Cybernetics

Problem Description

Based on previous results and experience from the student project [1], the candidate is to implement and build a prototype of a functioning actuator for a stabilized camera.

Assignment:
1)   Give an overview of the field of nano-UAVs.
2)   Derive a dynamic model of the UAV-system with actuator.
3)   Based on the conclusions of [1], design an actuator for stabilization of the camera.
4)   Design a circuit board for the electronics and implement the proposed controller structure on a microcontroller
5)   Test the system and compare with simulations.

[1] S. Kjenstad, One-gram stabiliaed pan/tilt microcamera, 5th year project, Department of Engineering Cybernetics, NTNU, 2009

Assignment given: 11. January 2010
Supervisor: Jan Tommy Gravdahl, ITK

Abstract

This thesis describes the design and creation of a system for stabilizing a camera mounted on a nano-UAV. A prototype voice coil actuator was produced, and Hall effect sensors were used to measure the angle of the actuator. The actuator and sensor is used to counter vibrations in the UAV. A circuit board used to control the actuator was designed and created, and a controller for the system was implemented.

Testing showed that the controller was able to counter vibrations, but the bandwidth was low, only a few hertz. Wires connected to the actuator and sensor had significant impact on the system. They caused a spring/damper effect which meant more current was required, which again caused lower bandwidth due to saturation. On the other hand, the wires also lead to passive damping of higher frequencies. Unfortunately, there is a frequency band around 10 Hz where neither active nor passive control provides damping.

Preface

This master thesis was written during the last semester of the Master of Science degree in Engineering Cybernetics at Norwegian University of Science and Technology (NTNU). The thesis was written in cooperation with Prox Dynamics.

First of all, I would like to thank my supervisor, professor Jan Tommy Gravdahl, for his invaluable help and guidance during the work with this thesis. I would also like to thank Prox Dynamics for providing such an interesting assignment, and the people at Prox for their help: Pål Hagh Sandberg, Jørgen Syvertsen, and especially my co-supervisor Trygve Marton have given me invaluable help with this assignment.

I would also like to thank John Olav Horrigmo at Department of Engineering Cybernetics for his help with circuit board production and soldering.

Contents

List of Figures

Chapter 1

Introduction

1.1 Motivation

The company Prox Dynamics develops tiny Unmanned Aerial Vehicles (UAVs) for surveillance and reconnaissance. A camera is mounted on these UAVs to provide images for navigation and image analysis purposes. Due to turbulence, resonance etc., there are vibrations in the UAV. These cause individual images from the camera to become blurry, and the video sequence to shake between consecutive frames. A stabilized[1] camera that can counteract these vibrations will improve image and video quality and ease the usage of the UAV for the operator.

1.2 Problem Formulation and System Description

The nano-UAV has a camera with specifications given in Table 1.1.

Table 1.1: Camera specifications

Name	Value
Mass	0.1 g
Resolution	640×480
Field of view (diagonally)	80°
Field of view per pixel	0.1°

---

[1]Stabilized in this context means stabilizing as in image stabilization, i.e. removing vibrations from the image, not as in stability theory of systems.

Due to the tiny size of the nano-UAV, the total size of the camera stabilization system, including the camera, must be limited to 1 g. That means that the actuators, sensors and all electronics required to control the camera must have a mass of less than 0.9 g. The camera should be stabilized around two axes, pan (yaw) and tilt (pitch).

The vibrations in the UAV are concentrated around a few frequency bands. The first is due to turbulence, which produces vibrations of up to a few Hz. The second type comes from interactions between the rotor and the helicopter body. When these are connected rigidly, a resonance causes vibrations with a frequency around 10 Hz. The last type is caused by rotor vibrations, and is around the rotor frequency of 85 Hz and multiples thereof. The amplitude of the vibrations is highest at the low frequencies. At 1 Hz, the amplitude is up to $\pm 30°$, this is reduced by 6 dB per octave.

The task of this work is to create a larger scale prototype of this camera stabilization system. The prototype will be limited to one axis, and will be about 10 times as large as the size requirement in the final system.

1.3 Previous Work

This master's thesis is a continuation of my final year project [18]. In that project, various solutions for stabilizing a camera were considered. Active control, using voice coil actuators and Hall effect sensors were chosen as the best solution. A model of the system was developed and the system was simulated using various controllers. Unfortunately, there was an error in the model developed in that project. The simulations were therefore done using an erroneous model, and do therefore not reflect the situation in reality very well. Even though the simulations were wrong, other parts of the work done in the project thesis can still be used in this master's thesis. The ideas regarding actuators and sensors will be used in this thesis.

As this thesis is built upon the final year project, some of its content is copied in this thesis. Chapter 2 is taken directly from [18]. The first half of Chapter 5 is based upon the similar chapter in [18], but some changes have been made. Smaller parts of Chapter 3 and Chapter 6 are also taken from [18].

1.4 Structure of the Thesis

Chapter 2 gives an overview of nano-UAVs, their usage and challenges in their development.

Chapter 3 presents the mechanical design of the system, including the voice coil actuator and Hall effect sensor.

Chapter 4 considers circuit board design, and presents the choices that were done regarding component selection etc.

Chapter 5 derives the model of the system, and explains how the parameters in the model are found.

Chapter 6 explains various concepts used in the controller, and also explains how the controller is implemented.

Chapter 7 describes how the system was tested and presents the test results. It also presents some of the simulation results from the project thesis using the fixed model.

Chapter 8 provides a discussion of the results, and on the challenges of further miniaturization.

Chapter 9 presents the conclusions of this work and give an overview of the further work that needs to be done.

Chapter 2

Nano Air Vehicles[1]

In 2005, the US Defense Advanced Research Projects Agency (DARPA) issued a challenge to produce a Nano Air Vehicle (NAV) [28]. The challenge was to build an unmanned air vehicle with a mass less than 10 g, including a 2 g payload, and less than 5 cm in any dimension. The NAV should have a top speed of $7 - 10$ m/s, and be able to fly up to 1000 m. This is an improvement over an earlier DARPA project with the goal of making Micro Air Vehicles (MAV) with dimensions of less than 15 cm, and a mass of around 200 g.

2.1   Applications

The main military application for UAVs today is Intelligence, Surveillance and Reconnaissance (ISR) missions [12]. Due to their size, nano-UAVs will be able to operate in areas where larger UAVs cannot, such as inside buildings, caves or tunnels [28]. The small size also means that they are easy to carry for soldiers, and can be used whenever a soldier requires information about the surroundings. This can be, for example, to see what is behind a corner, to get an overview of an area, or to check out a suspicious object [22]. The size of the UAV provides natural stealth, so the nano-UAV can do its work unnoticed while the soldier is located in a safe place.

The stealth of the nano-UAV can also make it suitable for attack. They can be loaded with small amounts of explosives to take out strategically important targets, such as power grid, command nodes, enemy air defense, aircraft on the ground, or enemy snipers [12].

The nano-UAVs available today are remote controlled, but in the future they may become completely autonomous. This will allow an operator to

---

[1]This chapter was written in cooperation with Sigurd Hannaas

set a mission, and then do something else while the UAV finishes its mission on its own. With autonomous operation, it may also be possible for several UAVs to operate together in a swarm. Davis [12] gives a potential scenario where 50 tiny UAVs are released and work together to take out a sniper.

Nano-UAVs can also be useful in civilian surveillance applications. The fact that they can be used indoors and around obstacles means that they can be used for reconnaissance in the case of accidents or in dangerous environments such as nuclear facilities or chemical plants. Their portability is useful for emergency services or law enforcement officers whenever information about an object or an area is required but getting close to that object is undesired.

2.2   Structural Topologies

The DARPA nano-UAV specifications do not specify what kind of aircraft will be most suited for the task. In both academic as well as commercial research, there is currently a lot of different design proposals to fulfill the requirements (or at least some of them), such as traditional fixed-wing aircraft, ornithopters (aircraft flapping its wings like a bird or an insect) and rotary-wing aircraft. The different approaches have various advantages and disadvantages.

Ornithopters offer great miniaturization possibilities (there exists flying prototypes weighing in at about one gram [21]) and seem to have great maneuverability potential, but they are generally on a very early stage of development, and are currently inferior to the other structural topologies in terms of flight time and payload capability [11]. The flapping wings also produce significant movements in the body, complicating the use of vibration-sensitive payloads such as a video camera. Fixed-wing aircraft offer the best flight range-to-weight ratio, at the cost of poor hovering and low speed capabilities, and thus the ability to fly indoors.

There exist numerous rotary-wing configurations, e.g. platforms with two or more rotors positioned side by side, helicopters with counter-rotating rotors placed on top of each other, and miniaturized traditional helicopters with only one main rotor to produce lift and a tail rotor to compensate yaw torque. The advantages of side-by-side-rotor platforms is the inherent torque compensation (as long as the aircraft is designed with this capability), rendering a tail rotor obsolete. In addition, the lift-to-weight ratio can be high, enabling big payloads. However, when considering miniaturization possibilities, these platforms have a disadvantage in that they need two or more equal main rotors, making the minimal sphere in which they could fit have a ra-

dius at least double that of the rotor radius. In addition, lift-producing rotors need powerful motors, adding considerable weight in itself, as well as having a large impact on power consumption, making heavier batteries necessary. These issues make this design unsuitable for the very smallest UAVs.

Helicopters with counter-rotating rotors on top of each other solve the size problem by stacking the rotors. These aircrafts do not need a tail rotor for torque compensation either, but would need one in order to turn while hovering. Otherwise there would be a need for complicated and heavy mechanics to render different rotational speeds on the two rotors possible, as a means of producing yaw moment on the body. Tail rotor or not, these aircraft need gears to produce the counter-rotating motion, adding weight and friction, and possibly more importantly for military applications, noise from the gears.

A method of fulfilling the requirements concerning maneuverability and weight/size is to base the design on a traditional helicopter layout. This layout will inherently have better miniaturization potential and flight endurance-to-weight ratio, compared to a multi-rotor platform, while retaining the latter's maneuverability and hovering capabilities. The helicopter has a disadvantage in that it needs to consume power in the tail rotor (which also adds weight and noise) just to compensate the torque produced by the main motor, and so it typically will have a lower lift-to-weight ratio. In addition it cannot have the same range-to-weight ratio as a fixed-wing aircraft, as it must actively produce all the necessary lift whenever airborne, whereas the fixed-wing aircraft only needs to compensate drag once sufficient airspeed is achieved. All these things considered, the traditional helicopter layout seems a good compromise between range and maneuverability, and thus a well suited layout to fulfill the nano-UAV requirements. The Prox Dynamics UAV, which is the subject of this text, is an aircraft of this kind, and therefore the rest of this chapter will only consider this specific layout whenever topological issues are discussed.

2.3   Technological Challenges

An important issue when discussing nano-UAVs is their power-to-weight ratio. A considerable part of the weight budget is occupied by the battery, and the battery's energy density (energy per mass) is the essential parameter in this context. The energy density has increased by a factor of 3.8 [20, Table 1] from the Nickel Cadmium batteries of 1990 (36.59 Wh/kg) to the Lithium-Polymer kind from 2007 (139.88 Wh/kg). A higher energy density enables longer flight times and lighter aircraft. In the future, even more energy-dense

Figure 2.1: Prox Dynamics nano-UAV

battery technologies will probably come into existence, making aircraft with even lower weight and better endurance than today possible.

A hovering aircraft must actively produce all its lift and must therefore have a relatively powerful main motor. Electrical motors contain heavy materials such as copper windings, so in the process of miniaturization, different designs have been suggested. A brushed DC motor with a gearbox typically has a lower power-to-weight ratio than a brushless motor with a similar gearbox and at similar speeds [20, Chapter III]. In addition, the brushed motor will experience wear on the brushes, and so need more frequent maintenance or replacement. If the brushless motor is turned "inside-out", with the permanent magnet rotor enclosing the stator, the gearbox can be removed due to the high-torque properties of such outrunner-motors at these speeds, making the outrunner brushless permanent magnet motor best of the three in terms of power to weight. Even though electrical motors are well understood and a highly developed branch of technology, miniaturization poses new and unexplored challenges. There is a lack of knowledge on what effects the miniaturization may cause, so future research will probably come up with new and even more efficient motor designs.

A highly autonomous aircraft will need a lot of electronics for sensory equipment, communication, flight control and general avionic purposes. In recent years, more and more components have been compressed into a single chip, making the necessary electronics lighter and smaller. Communication

needs to be efficient in terms of power usage, range, antenna size and data density on the link (compression). Although a lot of improvement has been made, there is still work to be done and progress to be made.

Nano-UAVs operate in an environment similar to that of a small bird or an insect, that is, with a low Reynolds number. The aerodynamics in this environment is significantly different from that of a traditionally sized aircraft, so the design of airfoils etc. must be very different from the full-size design to obtain maximum efficiency. Research in this area will probably be able to produce very efficient airfoils in the future, which together with miniaturization development in the aforementioned research fields might enable very small and efficient aircraft with new and radical designs.

Chapter 3

Actuator and Sensor

In [18], various actuator and sensor technologies were considered. Voice coil actuators and Hall effect sensors were found to be most suitable on the small scales required in the nano-UAV.

In order to test the feasibility of using such a system to stabilize the camera, a larger scale prototype of this system will be created.

3.1 Voice Coil Actuator

A voice coil actuator (also known as a Lorentz force actuator) will be used to move the camera. The Lorentz force on a piece of conductor l with a current i through it, in a magnetic field $\mathbf{B}$ is [27]

$$\mathbf{F} = i\mathbf{B}(\mathbf{l}) \times \mathbf{l} \tag{3.1}$$

This means that the magnitude of the Lorentz force on a coil is dependent on the strength of the magnetic field, the length of wire affected by the field, and the current through the coil. When designing the actuator it is therefore possible to make some trade-offs between size and current consumption. The direction of the force is perpendicular to both the magnetic field and the current.

A coil can move in two different directions, shown in Figure 3.1. The Lorentz force can make the coil move in both of these directions, depending on the magnetic field configuration. If magnets are positioned in such a way that the magnetic field points inwards towards the center of the coil, the force generated will be in the direction marked as y in Figure 3.1.

The other option is to move the coil in the direction marked as x. In order to do so, the magnets must be positioned in such a way that the magnetic field points up on one side of the coil and down on the other.
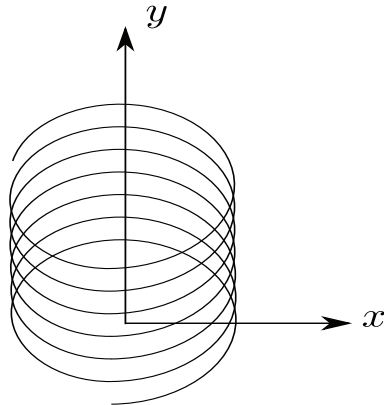
Figure 3.1: Directions of a coil

Both options can be used to make an angular voice coil [16]. Figure 3.2 shows the layout of both types. As no names are commonly given for these types, they will be called Type A and Type B in this thesis. Type A produces a force in direction y, while type B produces a force in direction x.

(a) Type A, top view

(b) Type B, top view

(c) Type A, side view

(d) Type B, side view
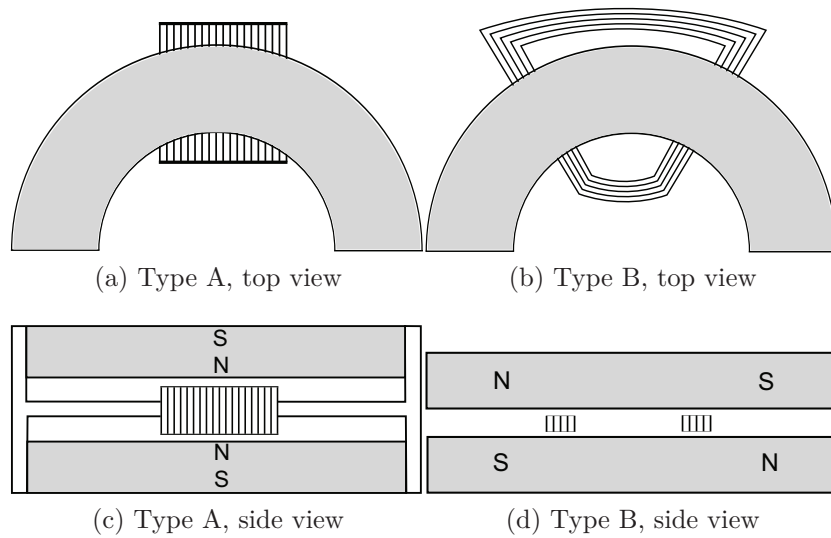
Figure 3.2: The two different configurations of angular voice coil actuators

A problem with type B is that the angle of rotation is limited. It will be very difficult, if not impossible to make an actuator of type B which can rotate more than 90°. For this reason it was decided to use an actuator of type A. A prototype was made by Prox Dynamics, which can be seen in Figure 3.3.
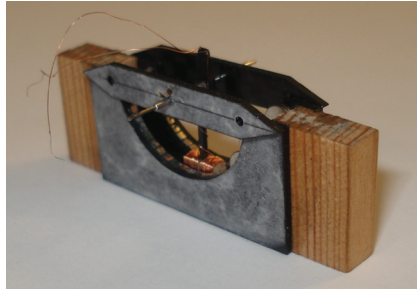
Figure 3.3: Prototype type A actuator

There were several problems with this actuator. The main problem was that the coil requires an iron core in order to close the magnetic circuit. However, including a core was difficult due to mechanical problems. The core must be made out of a magnetic material, which means it will be attracted by the magnets on the side of the coil. The only way of solving this problem is to make the construction very rigid, so that it the force from the magnets is too small to pull the coil towards the magnet. This is a viable approach for larger actuators, but on this scale, it is very difficult to create such a rigid construction. Without a core, the forces were very small, but not completely nonexistent.

A bent magnet like the one shown in Figure 3.2a and 3.2c is relatively uncommon, and will most likely have to be custom-made for this purpose. It was therefore decided to use several cubic magnets instead of one bent magnet. This introduces gaps between the magnets. These gaps cause the force to vary according to the angle, being high around the magnets, but very low at the gaps between magnets. Without a core, the force were small when the coil passed a magnet, but enough to move the coil. However, it stopped once it reached a gap, where the force was too low to move the coil.

Unlike the problem with the iron core, there are ways of solving this issue. One solution is simply to get a custom-made bent magnet. Another is to make an actuator consisting of a long bent coil and a short magnet, instead of the long magnet and short coil in this prototype.

As a type A actuator was not successful, it was instead decided to make an actuator of type B. This actuator was successful; a photo of it can be seen in Figure 3.4. This actuator has a mass of 3.66 g, and a maximum angle of about 50°. The mass is about 10 times as high as required for the final version. The UAV has vibrations with amplitude of up to ±30° at low frequencies, so in order to remove all vibrations from the camera, a maximum angle of 60° is required. This prototype will therefore not be able to stabilize the camera completely from the vibrations in the UAV. It should, however,
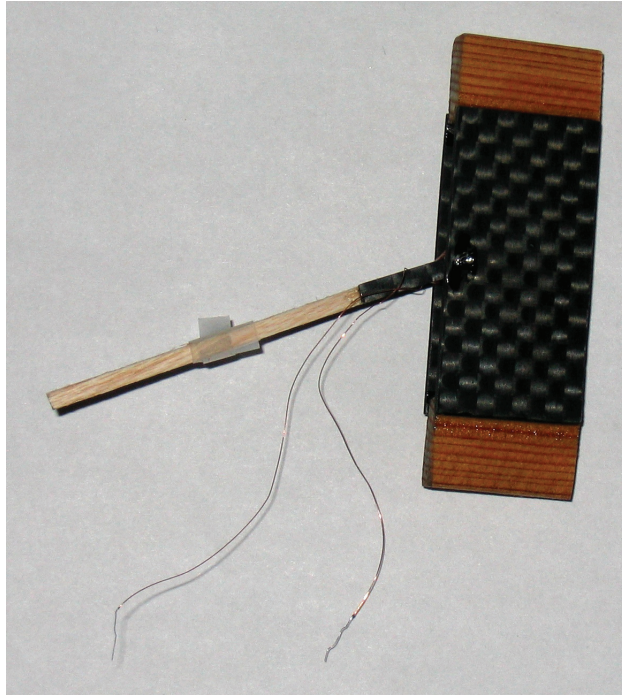
Figure 3.4: Actuator prototype

be possible to make an actuator of this type with a maximum angle of up to 90°, so a future version of the actuator may be able to stabilize all vibrations. For the tilt-axis actuator, it is desirable to be able to set the setpoint of the actuator to any angle within 90°. In order to do so, a total angle of 150° is required, which an actuator of type B is not able to handle.

Some changes were made in order to ease the construction, but the concept remains the same as shown in Figure 3.2b and 3.2d. Figure 3.5 shows a schematic of the actuator after these changes. One difference is that two cubic magnets are used instead of a bent magnet along the entire angle. This works for the relatively small angle of the prototype. If the angle is later increased to 90°, it may no longer be possible to use two magnets. The gap between the magnets may become too large to produce a force on the coil at all angles. Another difference is that the magnet on one side of the coil is removed and replaced by a metal piece connected to the other magnet. The metal piece keeps the magnetic circuit closed, while reducing the number of magnets required.

14

(a) Top view

(b) Side view
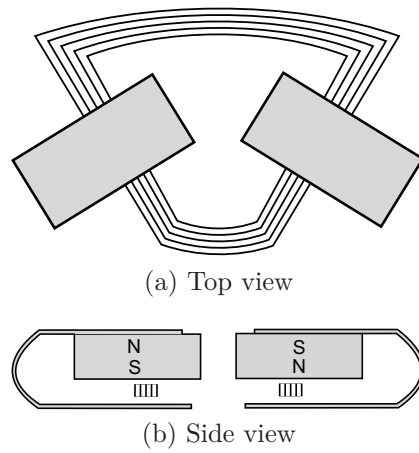
Figure 3.5: Schematic of actuator prototype

3.1.1   Two Axes

The goal is to stabilize the camera around two axes, pan and tilt, but as a prototype, only one axis was created. When a final version of this system is realized, it will include two axes combined somewhat like in Figure 3.6. The figure shows actuators of type A, but the idea should be the same if type B actuators are used.
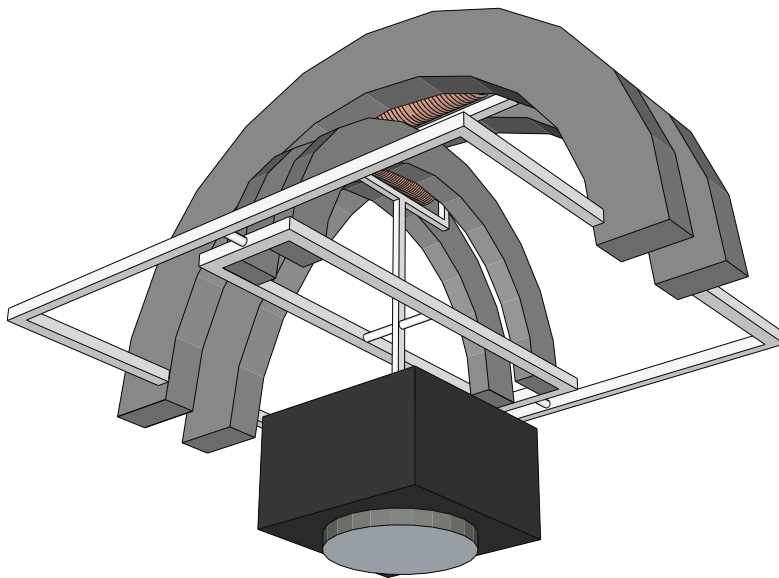
Figure 3.6: Two axes camera stabilization

3.2   Hall Effect Sensor
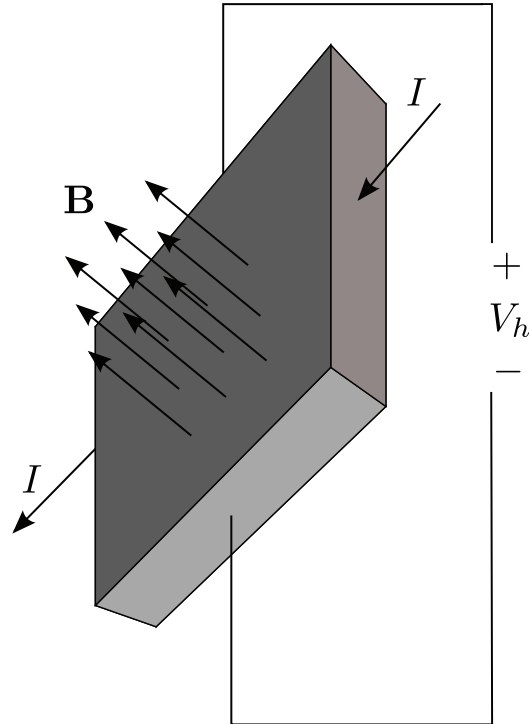
Figure 3.7: The Hall effect

A Hall effect sensor is a magnetic field sensor. When current flows through a conductor, and there is a magnetic field perpendicular to the current (see Figure 3.7), a voltage perpendicular to both the current and the magnetic field is produced. This voltage is given by [27] as

$$V_h = \frac{I}{nte}B \tag{3.2}$$

where I is the current through the conductor, t is the thickness of the conductor, e is the electron charge, and n is the carrier charge density of the electrons. nte is a constant for a given sensor. If the current I is kept constant, the Hall voltage V_h will be proportional to the magnetic field.

In order to use the Hall effect sensor as a position sensor, permanent magnets must be placed on the stationary part of the actuator, while a Hall effect sensor is placed on the moving part (or vice versa). The magnetic field will be different at different places around the magnet, so there is a relationship between the position of the sensor and the magnetic field measured. In a

voice coil actuator, there are already permanent magnets present. Depending on the actuator configuration, these may also be used as the permanent magnets for the sensor, so that no extra magnets are required

For actuator type A, the magnetic field is relatively constant over the entire path where the coil travels. Actuator type A will therefore most likely require additional magnets in order to measure position. Actuator type B, on the other hand, has two magnets with opposite polarities along the path of travel. This means the magnetic field will vary along the angle.

If the sensor was mounted on the coil, directly underneath the magnets, the output of the sensor would have been like the one described as Bipolar slide-by mode in [17], i.e. a sinusoid. In order to make the torque as high as possible, the air gap between the magnet and the coil should be as low as possible. Mounting the sensor directly underneath the magnet means that the air gap must increase in order to make room for the sensor. Instead, the sensor will be mounted in front of the magnets, like shown in Figure 3.8. Tests showed that the output from the sensor as a function of position is similar to what it would have been if the sensor were directly underneath the magnets.
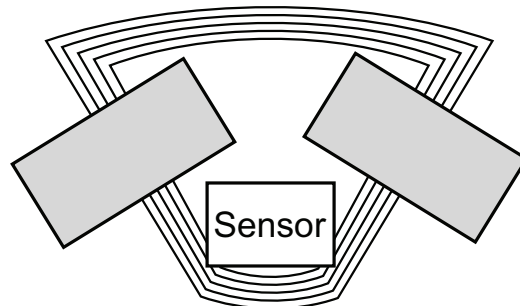
Figure 3.8: Sensor mounting

The maximum and minimum of the field-position function is when the sensor passes by the magnetic poles. As long as the sensor stays between the magnetic poles there will be a one-to-one correspondence between the magnetic field and the position. For the prototype actuator, the sensor is always between the poles, but if the maximum angle is increased to closer to 90°, it may be necessary to place the magnets so that the Hall effect sensor can travel outside the magnetic poles.

When there is a one-to-one correspondence, finding the position is simply a matter of inverting the field-position function. However, only the fact that the function is a sinusoid is known, the exact function is not. An approximation is done by measuring the angle for a number of equally spaced output voltage levels. The position is then calculated by finding the two nearest voltage levels to the measured voltage, and using linear interpolation between those two levels.

When current flows through the coil, it becomes an electromagnet and produces a magnetic field. The Hall effect sensor will thus not only measure the magnetic field from the permanent magnets but also the magnetic field from the coil. However, when measuring the output from the sensor at the same angle with and without current through the coil, no difference at all was seen in the output from the sensor. It can therefore be concluded that the magnetic field produced by the coil is insignificant compared to the magnetic field of the permanent magnets.

The Hall effect sensor needs to be small, not only due to the weight requirements of the UAV, but also due to the fact that it must be mounted on the moving part of the actuator. A higher mass means a higher moment of inertia which is undesirable because a larger actuator or higher power is required to move the moving part. Also, a sensor with larger volume will be more difficult to mount on a small actuator without interfering with the rest of the actuator.

The smallest package available for Hall effect sensors are the Allegro Microsystems A139x series [1]. The different values of x indicate different sensitivities. The size of these sensors are 3x2x0.75 mm [1], and their mass is 0.0136 g [2]. These sensors contain the Hall element and all necessary circuitry to produce a voltage proportional to the magnetic field strength.

It is possible to find even smaller packages containing just the Hall element without any external circuitry, for example Asahi Kasei HG-0111 [5], whose dimensions are 1.6x0.8x0.5 mm. However, these require additional external circuitry, at least an amplification circuit, so the total mass will be larger. These external components can be placed on a circuit board outside the actuator, so if the space to mount the sensor is very limited, this may be an alternative. On the prototype actuator, there is enough space for an A139x, so that sensor will be used. Later, when the actuator is miniaturized, switching to a smaller package with just the Hall element may be considered, if there is not enough room for an A139x sensor.

The minimum difference in magnetic field measurable depends on the sensitivity of the sensor and the resolution of the A/D-converter. The resolution of the A/D-converter is generally fixed. For example, for Atmel microcontrollers it is 10 bits. Hall effect sensors exist with many different sensitivity

values. With higher sensitivity values it is possible to measure smaller difference in magnetic fields, but since the maximum output voltage is the same, the maximum field strength measurable is reduced. The minimum value that can be measured with a sensor with a sensitivity of s V/T with a b bit A/D-converter is

$$\Delta B_{min} = \frac{V_{CC}}{s2^b} \tag{3.3}$$

The Allegro Microsystems A139x series of hall effect sensors come with different sensitivities, from 1.25 mV/G to 10 mV/G (12.5 V/T to 100 V/T). The magnetic field in the actuator is fairly small, so the most sensitive version (A1395 with a sensitivity of 10 mV/G) is chosen.

With this sensor and the 10-bit A/D-converter of Atmel microcontrollers, the minimum magnetic field measurable is 50 µT.

The sensor was mounted on the moving part of the actuator, close to the magnets. The output voltage from the sensor ranged from 1.1 V to 2.3 V when the sensor moves from one extreme angle to the other. This corresponds to a magnetic field ranging from -8 mT to 10 mT.

3.3 Wires

The wires connected to the moving part of the actuator will have a significant effect on the behavior of the system. These wires have the effect of a spring and damper. The spring effect means that additional torque is required to stabilize the camera, especially for vibrations with high amplitude. The torque from the actuator will not only be used to accelerate the actuator, but also to overcome the torque from the wires.

The effect of the wires is difficult to model correctly. The effect is not completely linear; there are nonlinear effects as well as the spring/damper effect. And even the linear effect is difficult to model correctly because measurements of the spring and damper constant will most likely be inaccurate. This will be discussed in more detail in Chapter 5.

3.3.1   Passive Damping

The spring/damper effect of the wires may also be a positive thing, as it gives the system passive damping of higher frequencies.
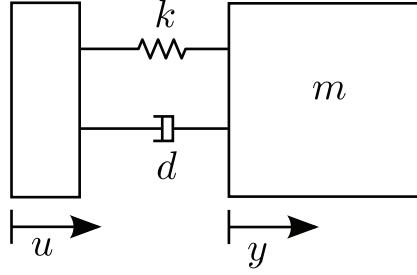

Figure 3.9: Passive stabilization

A passive stabilization system can be modeled as a system where one vibrating object is connected to another. If they were rigidly connected, all of the vibrations of the first object would be transferred to the second. However, if they are connected through a spring and a damper, as seen in Figure 3.9 for the linear case, the high frequencies of the vibrations will not be transferred. In Figure 3.9, u is the position of the object that forces the vibrations, and y is the position of the object that receives the vibrations. k is the spring constant, d is the damping constant and m is the mass of the object that receives the vibrations. The equation for this system is [13]

$$m\ddot{y} + d\dot{y} + ky = d\dot{u} + ku \tag{3.4}$$

In this case, the vibrations have angular motion, not linear. The equation then becomes

$$J\ddot{\theta}_o + d\dot{\theta}_o + k\theta_o = d\dot{\theta}_h + k\theta_h \tag{3.5}$$

Here, θ_h is the angle of the helicopter relative to the environment which corresponds to u in equation 3.4. Similarly, θ_o is the angle of the camera, this also relative to the environment.

The Laplace transform of Equation (3.5) gives the following transfer function from the helicopter vibrations to the camera vibrations:

$$\frac{\theta_o}{\theta_h}(s) = \frac{d}{J}\frac{s + \frac{k}{d}}{s^2 + \frac{d}{J}s + \frac{k}{J}} \tag{3.6}$$

If the camera is attached to the helicopter body using a spring with spring constant $k = 5.5 \cdot 10^{-5}$, damping $d = 10^{-5}$ and the moment of inertia is $J = 2 \cdot 10^{-7}$ (See Section 5.4 for why these values are used), the frequency response

Bode Diagram
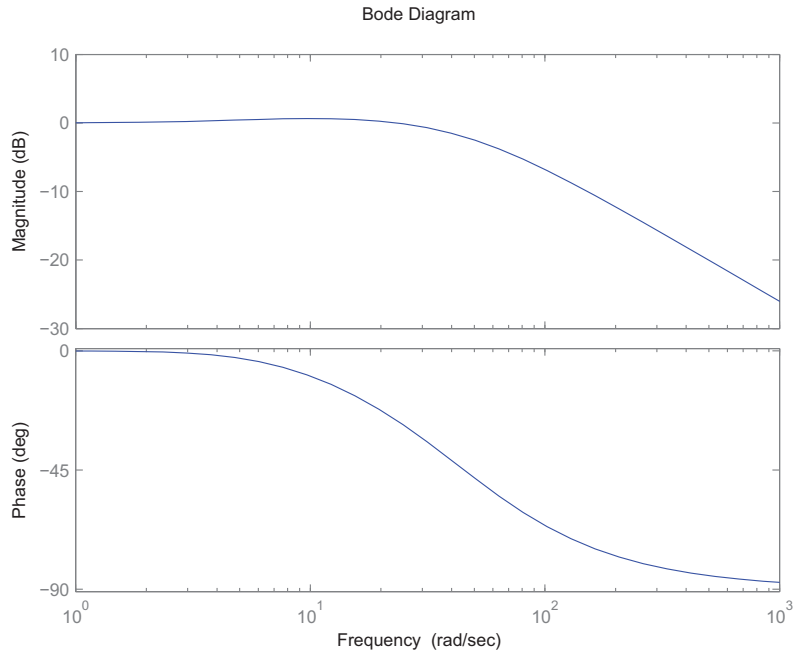
Figure 3.10: Bode plot of passive stabilization

of the passive vibration damping will be as shown in Figure 3.10. This shows that the wires provide passive damping at frequencies from around 6 Hz and up.

As passive stabilization only provides damping at high frequencies, it is unsuitable on its own. But as the active control is only good at low frequencies, passive stabilization may provide damping at frequencies higher than the bandwidth of the active control.

Chapter 4

Circuit Board Design

A circuit board was designed and created in order to host all the integrated circuits (ICs) and other components required to stabilize the camera. The circuit board also contains components used for testing and debugging the system. As this is only a prototype, it will not be miniaturized, but when choosing the components, some thought will be given to their size in order to make miniaturization easier when the final system will be created. The circuit board was designed with two-axis stabilization in mind, but as only one actuator prototype was created, only one of the axes was used.

4.1 Components

4.1.1 Gyro

The reference angle for the camera is the angle of the UAV relative to the environment. This angle is measured by gyroscopic sensors already part of the UAV, and will not be part of the camera subsystem. In order to test the camera stabilization without the UAV, gyroscopic sensors are also mounted on the circuit board.

All gyros have a maximum angular velocity which they are able to measure. The maximum angular velocity can be found by looking at the frequency distribution of the helicopter vibrations. Though it will be hard to generate vibrations with a similar frequency distribution outside of the UAV, the choice of gyro will still be based on that frequency distribution. The amplitude of vibrations is reduced by 6 dB per octave, which means that the maximum angular velocity is the same at all frequencies. The angular velocity will therefore be calculated at 1 Hz, where the maximum angular

displacement is $\pm 30°$:

$$
\begin{aligned}
\omega_{max} &= \max \frac{\mathrm{d}}{\mathrm{d}t}(30\sin(2\pi t)) \\
&= \max(30 \cdot 2\pi \cos(2\pi t)) = 30 \cdot 2\pi = 188°/\mathrm{s}
\end{aligned}
\tag{4.1}
$$

The maximum angular velocity of the sensor must be higher than this, but preferably, it should not be much higher. The output from a sensor is an analog voltage between 0 and V_{CC}, where 0 indicates rotation at maximum angular velocity in one direction, while V_{CC} indicates rotation at maximum angular velocity in the other direction. If the maximum angular velocity of a gyro is high, the sensitivity of the gyro (mV/°/s) becomes lower. Therefore, it is desirable with a gyro with a maximum angular velocity just above required, in order to have as high sensitivity as possible.

The gyro chosen is LPY530AL from STMicroelectronics [25]. These are MEMS (microelectromechanical) gyroscopes, which utilizes the Coriolis effect to measure angular velocity [26]. The gyro contains two masses for each axis, oscillating in opposite directions. When the gyro rotates, the Coriolis effect generates a force on these masses proportional to the angular velocity. This force is measured by measuring the difference in capacitance between the two masses. This is used to create an output voltage proportional to the angular velocity. LPY530AL is a two-axis gyroscope, measuring rotation around both the pitch and yaw axes. It can measure a maximum angular velocity of 300°/s. This is the nearest value above 188°/s, which can be found in relatively cheap gyroscopic sensors. The gyro has a bandwidth limit of 140 Hz. This limit is imposed by an internal lowpass filter in the IC, in order to remove high frequent noise from the sensor output. This limits the bandwidth of the controller to the same frequency, as there is no way to measure higher frequencies.

4.1.2 Microcontroller

An Atmel ATMega128 microcontroller [7] will be used to control the system. This microcontroller contains 128 kB of flash memory, which is more than enough. It has all features required to control the actuator, such as timers, PWM output, and A/D converters. It comes in a 64 pin package, which is unnecessary large. Later, if this IC is found to be too large, one may replace it with a smaller 32 pin Atmel microcontroller, such as ATMega168. The code written for ATMega128 can be used on a different Atmel microcontroller without much change.

ATMega128 requires an external oscillator. An 8 MHz crystal is used for this purpose. Atmel microcontrollers can run as fast as 16 MHz, but only when the supply voltage is 5 V. The Hall effect sensors and the gyro requires a supply voltage of 3.3 V, so the entire circuit board uses 3.3 V as supply voltage. With a supply voltage of 3.3 V, the maximum clock frequency is 8 MHz. Several other Atmel microcontrollers come with its own internal 8 MHz RC oscillator, so if one later switches to e.g. ATMega168, the crystal can be dropped.

4.1.3   Motor Driver

Pulse Width Modulation (PWM) will be used to control the actuator. PWM is a square pulse which has a constant frequency and constant amplitude, but where the percentage of time where the signal is high can change. This percentage is called the duty cycle, and is used to determine the output voltage. If this signal is lowpass filtered, the output voltage over the entire period will be roughly equal to the average of the voltage, i.e.

$$V_{out} = V_{CC}d \tag{4.2}$$

where d is the duty cycle given as a percentage of the period. The RL circuit of the actuator (see Section 5.2.1) acts like a lowpass filter.

Due to the currents required to drive any actuator, it is not possible to drive it directly from the output of a microcontroller. Instead the signal from the microcontroller is used to switch another voltage (V_{CC}), which drives the actuator. In order to do so, an H-bridge is used.

An H-bridge can conceptually be described as in Figure 4.1 [10]. Actual implementation of an H-bridge is usually more complex. If transistors T_1 and T_4 are turned on, current flows from V_{CC} to ground through the motor one way. If, on the other hand, transistors T_2 and T_3 are turned on, current flows the other way through the motor. To set the voltage of the actuator to any value, one of the transistors are kept open, while the PWM signal from the microcontroller is used to switch the other one.

The motor driver used in this application is Allegro Microsystems A3901 [3]. This is an IC consisting of 2 H-bridges, enough to control both axes. It can handle switching frequencies of up to 250 kHz, which is far more than required. The current that this motor driver can handle is limited to 400 mA. When testing the controller (see Chapter 7) it was noted that this may be slightly too low. It may therefore be necessary to replace the motor driver with one that can handle higher currents. However, the required current may scale down with the size of the actuator, so it may not be a problem in the final system. See Chapter 8.2 for some discussion on scaling.
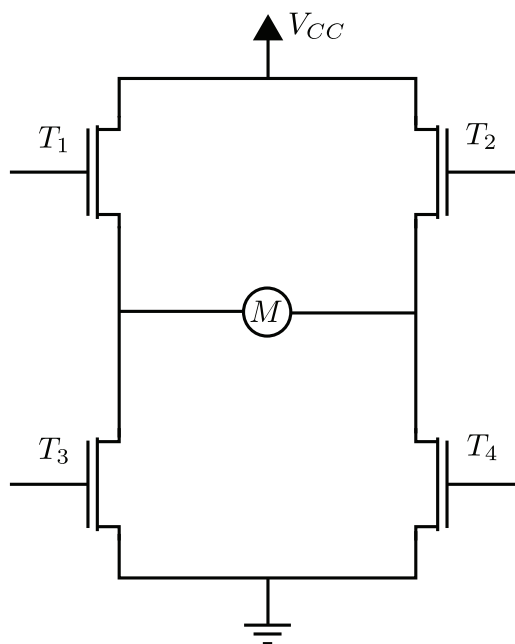
Figure 4.1: H-Bridge

4.1.4 Communication

To program and debug the microcontroller, JTAG [10] is used. JTAG requires nothing on the circuit board except for a connector. The circuit board must also be connected to a PC in order to write debug information, sensor measurements etc. UART [10] is used as the protocol for communicating with the PC. Future Technologies FT232R [14] is used to convert the UART data to a USB signal, and the circuit board is connected to a PC with a USB cable.

4.2 Production

EAGLE CAD software was used to draw the schematics for the circuit board. The required external components such as resistors and capacitors were found in the datasheets for the parts and placed according to those datasheets. This schematic can be seen in Figure A.1 and A.2. The same program was used to lay out the components and connections between them on a circuit board. This layout can be seen in Figure A.3. The circuit board was then produced by circuit board etching using equipment provided by Department of Engineering Cybernetics. Figure 4.2 shows the circuit board without any components on it. Finally, the components were soldered on; the result can
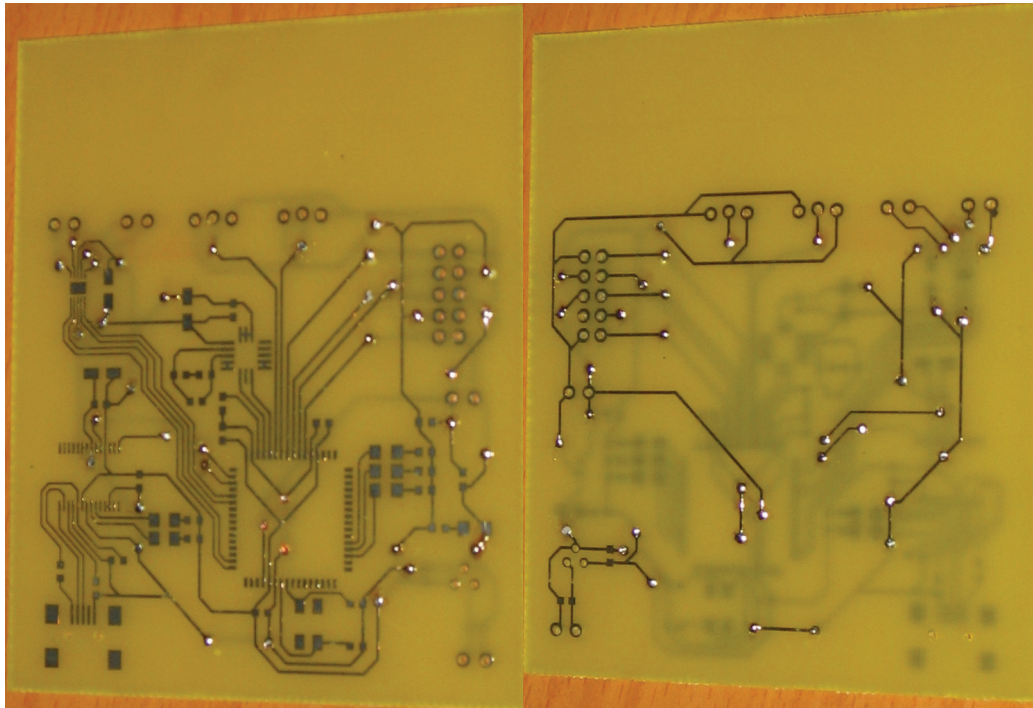
(a) Top

(b) Bottom

Figure 4.2: Empty Circuit Board

be seen in Figure 4.3.

4.3 Further Miniaturization

Most of the components that are on the circuit board for this prototype version can be removed in a miniaturized version of the system. There is no longer any need for gyro sensors, as gyros already exist on the UAV. Instead, some way of communicating with the rest of the UAV is required, but this should be no more than a few connectors. Debug output to a PC will no longer be required, which means the UART-to-USB converter and the USB connector can be removed. Programming of the microcontroller is done using a JTAG interface in this development board. This requires a 2x5 pin header, which can be removed if the microcontroller is programmed some other way, possibly outside of the circuit board before it is soldered on. That leaves only the microcontroller and the motor driver, plus the external components required by these ICs. The microcontroller can be replaced by a smaller 32-pin one, e.g. ATMega168. The smallest package available for this
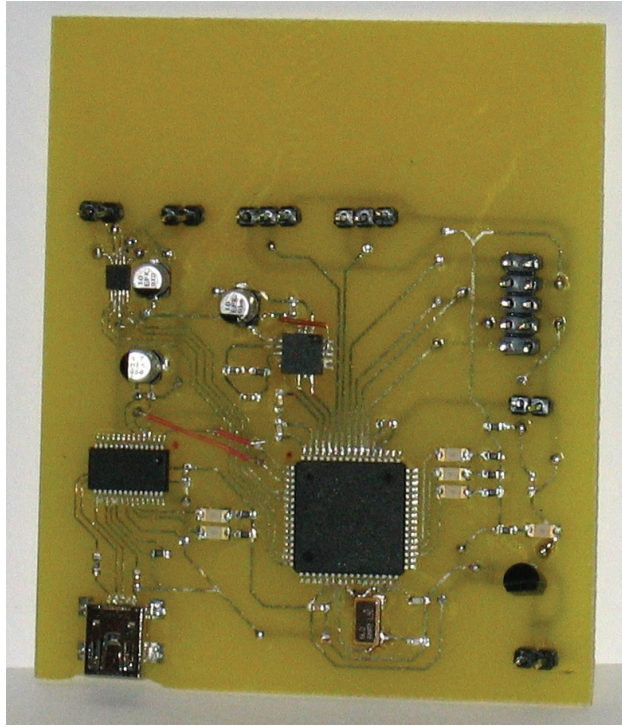
27

Figure 4.3: Circuit board with all components mounted

microcontroller has a mass of just 0.0654 g [6].

A summary of the ICs required in the final system (including the Hall effect sensors, which are not on the circuit board), and their mass is found in Table 4.1.

Table 4.1: Mass of suggested integrated circuits

Type	Name	Mass	Ref
Hall effect sensor	Allegro A1395	0.0136 g	[2]
Hall effect sensor	Allegro A1395	0.0136 g	[2]
Motor driver	Allegro A3901	0.0245 g	[4]
Microcontroller	Atmel ATMega168	0.0654 g	[6]
Sum		0.1171 g	

In addition to the components in Table 4.1, a few capacitors and resistors are required, plus the connectors and wires required to connect the circuit board to the actuator and to the rest of the UAV. The circuit board itself also adds mass to the system.

Chapter 5

Modeling

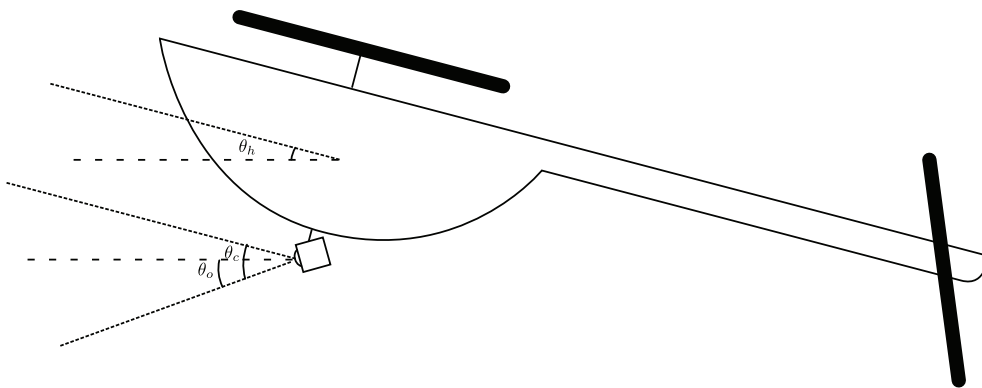## 5.1 Modeling of the Mechanical System

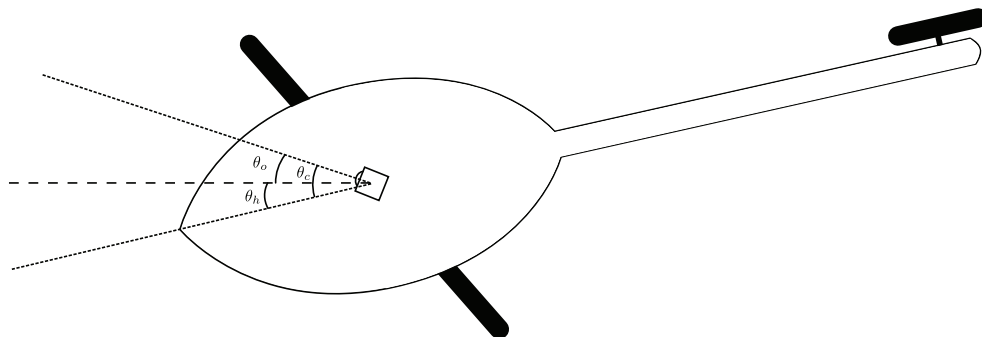Figure 5.1: Angle definitions for the tilt axis

Figure 5.2: Angle definitions for the pan axis

The angles used in the model are shown in Figure 5.1 and 5.2. For the tilt axis, θ_h is the angle between the helicopter body and the horizontal plane, θ_o is the angle between the camera and the horizontal plane, and $\theta_c = \theta_o - \theta_h$ is the angle between the helicopter body and the camera. The situation is similar for the pan axis, shown in Figure 5.2. θ_h and θ_o are in this case relative to an axis which is fixed with respect to the environment.

The fact that the camera angle, θ_c, is a rotation around a different point than the helicopter angle, θ_h does not matter. If the angle is controlled perfectly, this will only give an error in the linear motion of the camera. However, linear motion matters very little for camera stabilization [23], and is therefore ignored.

The equation of rotating motion around one axis is

$$\sum \tau = J\ddot{\theta}_c \tag{5.1}$$

where $\sum \tau$ is the sum of all torques that are acting on the system and J is the moment of inertia.

The torques that acts on the system are the input torques from the actuators (τ), the torque from the wires connected to the actuator (τ_w), the torques due to the friction (τ_f), and, if the center of mass is not at the rotation center, torques due to gravity (τ_g). That means the equation of motion is

$$\tau + \tau_w + \tau_f + \tau_g = J\ddot{\theta}_c \tag{5.2}$$

5.2 Modeling of a Voice Coil Actuator

The Lorentz force on a piece of conductor $\mathbf{l}$ in a magnetic field $\mathbf{B}$, with a current i through it, is [27]

$$d\mathbf{F} = i\mathbf{B}(\mathbf{l}) \times d\mathbf{l} \tag{5.3}$$

For a conductor of length L, the force is

$$\mathbf{F} = i \int_0^L \mathbf{B}(\mathbf{l}) \times d\mathbf{l} \tag{5.4}$$

The magnitude of this force in the direction of rotation is

$$F = i \int_0^L B(l) \cos(\phi(l)) dl \tag{5.5}$$

where ϕ is the angle between the magnetic field and the conductor. If the result of the integral is called K_e, the force on the entire coil can be written as

$$F = K_e i \tag{5.6}$$

If the actuator is a rotating actuator where the force is perpendicular to the rotation, the torque produced by the actuator is

$$\tau = Fr \tag{5.7}$$

where r is the radius from the center of rotation to the point where the force is applied. Inserting this into Equation (5.6) gives the torque equation for a rotating voice coil actuator:

$$\tau = K_e(\theta_c)ri \tag{5.8}$$

Here, K_e is written as a function of the angle θ_c. This is due to the fact that the magnetic field is not necessarily the same along the entire magnet, and therefore K_e may depend on the position of the coil in the magnetic field.
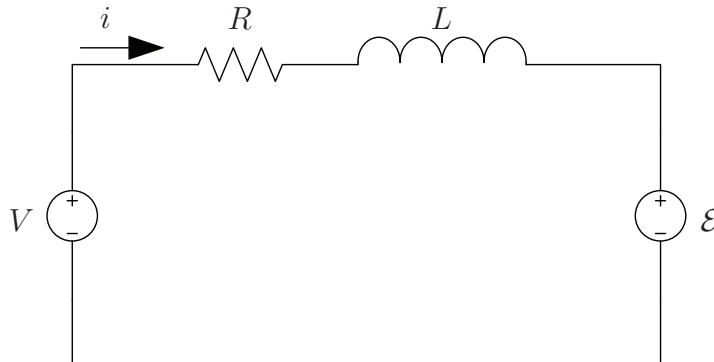
5.2.1 Electrical Circuit

Figure 5.3: Electrical circuit for the voice coil actuator

The electrical circuit of the voice coil can be modeled as shown in Figure 5.3. In this circuit, R and L are the resistance and inductance of the coil, V is the input voltage, i is the current through the circuit and $\mathcal{E}$ is the back-emf which is produced when the coil is moving through a magnetic field. Applying Kirchhoff's law around that circuit gives

$$V = L\frac{\mathrm{d}i}{\mathrm{d}t} + Ri + \mathcal{E} \tag{5.9}$$

The equation for $\mathcal{E}$ is [27]

$$\mathrm{d}\mathcal{E} = v\mathbf{B}(\mathbf{l}) \times \mathrm{d}\mathbf{l} \tag{5.10}$$

where v is the velocity of the moving part of the actuator. The term $\mathbf{B}(\mathbf{l}) \times \mathrm{d}\mathbf{l}$ in Equation (5.10) is the same as the similar term in Equation (5.3), so $\mathcal{E}$ can be calculated in the same way as the force of the actuator. $\mathcal{E}$ is then

$$\mathcal{E} = K_e(\theta_c)v = K_e(\theta_c)r\dot{\theta}_c \qquad (5.11)$$

Inserted into Equation (5.9), we get

$$V = L\frac{\mathrm{d}i}{\mathrm{d}t} + Ri + K_e(\theta_c)r\dot{\theta}_c \qquad (5.12)$$

5.2.2   Wires

The wires are acting on the system similar to a spring and damper. The torque produced by such a spring and damper system can be written as

$$\tau_w = -k_w\theta - d_w\dot{\theta} \qquad (5.13)$$

Measurements show that the wires do not behave exactly like a linear spring and damper, there are nonlinear effects as well. These nonlinear effects will be highly dependent on exactly how the wires are placed, and will be very difficult to model. Equation (5.13) is a good approximation, and is therefore used.

5.3   Complete System

Equation (5.2), (5.13), (5.8) and (5.12) describes the system. Together, they can be written as

$$\begin{aligned} J\ddot{\theta}_c &= K_e(\theta_c)ri + \tau_f + \tau_g - k_w\theta - d_w\dot{\theta} \\ V &= L\frac{\mathrm{d}i}{\mathrm{d}t} + Ri + K_e(\theta_c)r\dot{\theta}_c \end{aligned} \qquad (5.14)$$

By measuring K_e at different angles, it could be observed that K_e was independent of the angle. K_e is therefore considered constant in the model.

The mass of the moving part of the actuator is very close to symmetrical around the center of rotation. This means that the gravity forces act on both sides equally, and can therefore be ignored.

The friction effects are friction in the axle and air resistance. In order to make the model linear, viscous friction will be the only type of friction included in the model, $\tau_f = F_v\dot{\theta}_c$. Since viscous friction has the same equation as damping in the wires, it will not be possible to differentiate these two types of damping. They will therefore be combined into d_w.

This simplifies Equation (5.14) to

$$J\ddot{\theta}_c = K_e r i - k_w \theta - d_w \dot{\theta}$$

$$V = L\frac{\mathrm{d}i}{\mathrm{d}t} + Ri + K_e r \dot{\theta}_c$$

(5.15)

If we set the voltage as the input $u = V$, the position as the output $y = \theta_c$, and

$$x_1 = i$$
$$x_2 = \theta_c$$
$$x_3 = \dot{\theta}_c$$

as the states, we can write the system on a state-space form as

$$\dot{\mathbf{x}} = \mathbf{A}\mathbf{x} + \mathbf{B}u$$

$$\mathbf{y} = \mathbf{C}\mathbf{x}$$

(5.16)

with

$$\mathbf{A} = \begin{bmatrix} -\frac{R}{L} & 0 & -\frac{K_e r}{L} \\ 0 & 0 & 1 \\ \frac{K_e r}{J} & -\frac{k_w}{J} & -\frac{d_w}{J} \end{bmatrix}$$

$$\mathbf{B} = \begin{bmatrix} \frac{1}{L} \\ 0 \\ 0 \end{bmatrix}$$

(5.17)

$$\mathbf{C} = \begin{bmatrix} 0 & 1 & 0 \end{bmatrix}$$

As the controller must be implemented as a discrete controller on a microcontroller, the system must be discretized. This turns the system into

$$\mathbf{x}_{k+1} = \mathbf{A}_d\mathbf{x}_k + \mathbf{B}_d\mathbf{u}_k$$

$$\mathbf{y}_k = \mathbf{C}_d\mathbf{x}_k$$

(5.18)

where $\mathbf{A}_d$, $\mathbf{B}_d$ and $\mathbf{C}_d$ can be found by using the Matlab function `c2d`, with the matrices from Equation (5.17) as input.

5.4   Parameter Determination

In order to use a model based controller, the parameters of the model must be known. From Equation 5.14, it can be seen that the parameters of the model are resistance, inductance, radius, voice coil constant, moment of inertia and spring and damper constants from the wires. It would be preferable to have accurate measurements of all these parameters, but some of these parameters are difficult to measure.

Resistance

The resistance of the coil is measured by giving the actuator a constant voltage, measuring the stationary current, and then use Ohm's law to calculate the resistance. 1 V gave a current of 0.244 A, which means the resistance is

$$R = \frac{V}{I} = \frac{1}{0.244} = 4.1 \ \Omega \tag{5.19}$$

Inductance

Inductance is measured by looking at the time constant of the electric circuit. A small resistance is placed in series with the actuator, and the step response of the voltage over this resistance is measured using an oscilloscope. This step response has a time constant τ, and in an RL circuit, this time constant is $\tau = \frac{L}{R}$. R is in this case the total resistance, i.e. the resistance in the coil (measured previously), plus the series resistance, which is known to be 1 Ω. The measured time constant was 3.2 ms, which gives an inductance of

$$L = \tau R = 3.23 \cdot 10^{-3} \cdot 5.1 = 16.1 \ \text{mH} \tag{5.20}$$

Voice Coil Constant

The voice coil constant, K_e is measured by giving the actuator a constant current, and measuring the force at the end of the actuator arm. When supplying the actuator with a current of 0.3 A, the mass measured was 0.20 g, i.e. the force produced by the actuator is

$$F_s = mg = 0.20 \cdot 9.8 = 1.96 \cdot 10^{-3} \ \text{N} \tag{5.21}$$

The length of the arm is 4.95 cm which means the torque is

$$\tau = F_s l = 1.96 \cdot 10^{-3} \cdot 4.95 \cdot 10^{-2} = 9.70 \cdot 10^{-5} \ \text{Nm} \tag{5.22}$$

The magnets of the actuator produce a force at a radius of 1 cm from the center of rotation. This force is

$$F_r = \frac{\tau}{r} = \frac{9.70 \cdot 10^{-5}}{1 \cdot 10^{-2}} = 9.70 \cdot 10^{-3} \ \text{Nm} \tag{5.23}$$

From the fact that the current used was 0.3 A, the voice coil constant K_e is found to be

$$K_e = \frac{F_r}{I} = \frac{9.70 \cdot 10^{-3}}{0.3} = 3.2 \cdot 10^{-3} \ \text{N/A} \tag{5.24}$$

The force measured is the sum of all forces acting on the actuator. As explained in Section 3.3, the wires produce a significant force, acting like a spring. The spring force is dependent on the position of the spring relative to some zero point. If the force is measured with the actuator arm in the position where the spring produce no net force, all the forces measured are produced by the current. This was attempted, but as the positioning of the actuator on the weight was done by hand, it may have been inaccurate.

K_e may not be completely constant, but may be dependent on the angle of the actuator. However, such a dependence was not found. As the measurements were inaccurate, there may still be such a dependence, but it is lower than the measurement error. K_e is therefore considered a constant.

Moment of Inertia

The moment of inertia is difficult to measure, but can be estimated using the shape and size of the actuator. The shape of the actuator, however, is quite complex, and any estimate will therefore either be very complicated to calculate, or inaccurate. The mass of the moving part is also uncertain. No measurements were done before it was installed into the stationary part, and disassembling it was not possible. The moving part of the actuator consist of a 4.95 cm long rod on one side of the axis, and on the other side, a coil shaped roughly like a 35° sector of a circle with a radius of 1 cm. An estimate of the mass of the moving part is 0.5 g, with about half of it due to the rod and the other half due to the coil. The moment of inertia of a rod rotated around its end is [27]

$$J_{rod} = \frac{mL^2}{3} = \frac{0.25 \cdot 10^{-3} \cdot (4.95 \cdot 10^{-2})^2}{3} = 2.0 \cdot 10^{-7} \text{ kgm}^2 \qquad (5.25)$$

The coil has a moment of inertia of $\frac{35}{180}$ of that of a similar solid disk, which gives a moment of inertia of [27]

$$J_{coil} = \frac{35}{180} \frac{mr^2}{2} = \frac{35}{180} \frac{0.25 \cdot 10^{-3} \cdot (1 \cdot 10^{-2})^2}{2} = 2.4 \cdot 10^{-9} \text{ kgm}^2 \qquad (5.26)$$

This means that the moment of inertia of the coil is very small compared to that of the rod, and the total moment of inertia is

$$J = J_{rod} + J_{coil} = 2.0 \cdot 10^{-7} \text{ kgm}^2 \qquad (5.27)$$

Wire Spring Constant

In order to find the spring constant one can use the fact that $\tau = -k_w\theta$. A voltage of 1 V applied to the system, produces a current of

$$I = \frac{V}{R} = \frac{1}{4.1} = 0.24 \text{ A} \tag{5.28}$$

The torque from this current is

$$\tau = K_e r I = 0.24 \cdot 10^{-2} \cdot 0.0032 = 7.68 \text{ } \mu\text{Nm} \tag{5.29}$$

The angle measured with this voltage applied was -0.14 rad, which means that the spring constant is

$$k_w = -\frac{\tau}{\theta} = \frac{7.68 \cdot 10^{-6}}{0.14} = 55 \cdot 10^{-6} \tag{5.30}$$

As the wires are only approximated by a linear spring, this value cannot be considered accurate. The spring force also seems to change slightly over time as the wires move.

Damping

Measuring the damping constant was not possible, so the value was chosen by pure guesswork to be

$$d_w = 1 \cdot 10^{-5}$$

The damping seems to change significantly over time, so this value is inaccurate, at least for most of the tests made on the actuator.

Summary

The values of the parameters used in the model are summarized in Table 5.1. Of these parameters, only resistance, inductance and radius are close to accurate. The rest have various degrees of uncertainty.

Table 5.1: Actuator parameters

Name	Symbol	Value	Unit
Coil resistance	R	4.1	Ω
Coil inductance	L	$16.1 \cdot 10^{-3}$	H
Voice coil constant	K_e	$3.2 \cdot 10^{-3}$	N/A
Moment of inertia	J	$0.2 \cdot 10^{-6}$	kgm^2
Radius	r	$10 \cdot 10^{-3}$	m
Spring constant	k_w	$55 \cdot 10^{-6}$	Nm
Damping constant	d_w	$1 \cdot 10^{-5}$	Nms

Chapter 6

Control

A natural goal for the controller would be that the vibrations of the angle between the camera and environment (θ_o, see Figure 5.1) should correspond to less than one half pixel to each side, or one pixel peak to peak. Each pixel in the camera covers an angle of 0.1°, which means that the controller should ideally reduce the amplitude of all vibrations down to less than 0.05°. As the amplitude of the vibrations is reduced at higher frequencies, there is a point where the vibrations are less than $^1/_2$ pixel, above this frequency there is no point in reducing the frequency even more. This frequency is

$$f_{max} = \frac{30}{0.05} = 600 \text{ Hz}$$

Since 600Hz is not a multiple of the rotor frequency, the actual highest necessary bandwidth is the highest multiple of the rotor frequency below 600 Hz

$$f_{max} = 595 \text{ Hz}$$

From the frequency distribution of the vibrations, one can calculate that, in order to reduce the 1 Hz vibrations to less than $^1/_2$ pixel, the required damping is

$$|\frac{\theta_o}{\theta_h}(j2\pi \cdot 1)| = \frac{0.05}{30} = 20\log_{10}(\frac{0.05}{30}) \text{ dB} = -55.6 \text{ dB} \qquad (6.1)$$

At 10 Hz, the required damping is

$$|\frac{\theta_o}{\theta_h}(j2\pi \cdot 10)| = -55.6 \text{ dB} + 6\log_2(10) \text{ dB} = -35.6 \text{ dB} \qquad (6.2)$$

And similarly for multiples of the rotor frequencies:

$$|\frac{\theta_o}{\theta_h}(j2\pi \cdot 85N)| = -55.6 \text{ dB} + 6\log_2(85\text{N}) \text{ dB} \qquad (6.3)$$

It is unrealistic to make an active controller with a bandwidth this high, especially considering that the gyro can only measure frequencies up to 140 Hz. However, the wires provide passive stabilization at high frequencies, starting from about 6 Hz (see Figure 3.10). At the rotor frequency of 85 Hz, the passive stabilization provides a damping about 15 dB, slightly less than the required 17.1 dB, but almost good enough. At all higher multiples of the rotor frequencies, the wires provide enough passive stabilization for the amplitude θ_o to be less than $^1/_2$ pixel. At 10 Hz, the passive damping provide some damping, but only about 3.6 dB, which is nowhere near enough to stabilize the vibrations alone.
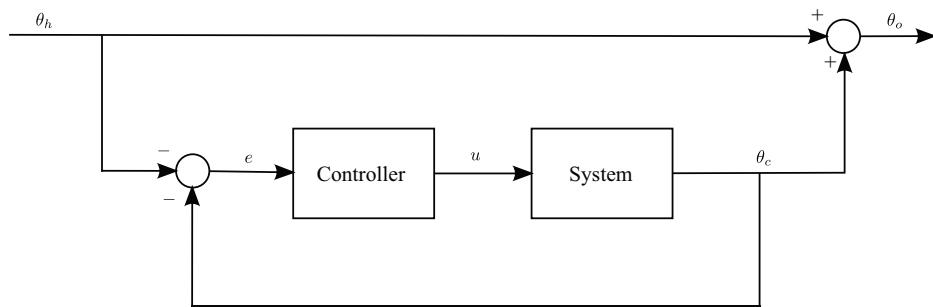
6.1   Controller Design

Figure 6.1: Block diagram of system with controller

The structure of the controller can be seen in Figure 6.1. The angle of the helicopter, measured by a gyro will be considered a reference which the controller will attempt to follow.

6.1.1   PID Controller

A Bode plot of the system, using the parameters found in Section 5.4 can be seen in Figure 6.2. In order for the system to be stable, the gain must be lower than 0 for all frequencies where the phase is less than $-180°$ [8]. Using a pure proportional controller, one can increase the gain so that it goes below zero just before ω_{180}. This controller will have a bandwidth of slightly less than ω_{180}, i.e. about 15 Hz.

Using a controller without integral action causes steady-state error. Due to the spring effect of the wires, this steady-state error can be quite significant. Integral action prevents steady-state error, but at the same time reduces the stability properties of the system. Integral action gives an extra
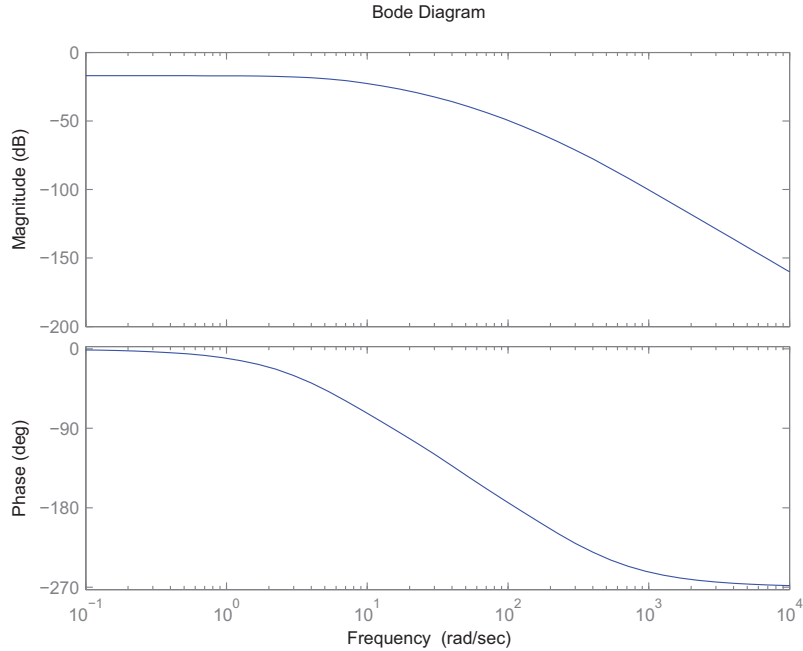
Figure 6.2: Bode plot of system

$-90°$ to the phase. ω_{180} will therefore be reduced to about 2.4 Hz, so when using a PI controller, the bandwidth must be lower than this.

In order to increase the bandwidth, the phase must be increased, and to do so, derivative action must be used. However, taking the derivative amplifies noise, so numerical differentiation cannot be used.

6.1.2 Kalman Filter

The measurements from the Hall effect sensor are noisy. As explained earlier, derivative action is required for fast control, but derivative action amplifies the measurement noise. In order to reduce the noise from the sensors, a Kalman filter is used. The Kalman filter, as explained in [9], is a state estimator which produces estimates of the state of a system without noise. One of the states in the system (x_3) is the derivative of the position. Feedback from the estimate of this state can be used instead of numerical differentiation as a way of including derivative action in the controller.

Given the system

$$\begin{aligned}
\mathbf{x}_{k+1} &= \mathbf{A}_d\mathbf{x}_k + \mathbf{B}_d\mathbf{u}_k + \mathbf{w}_k \\
\mathbf{y}_k &= \mathbf{C}_d\mathbf{x}_k + \mathbf{v}_k
\end{aligned} \tag{6.4}$$

$\mathbf{w}_k$ is the process disturbance and $\mathbf{v}_k$ is measurement noise. The covariance of $\mathbf{w}_k$ and $\mathbf{v}_k$ are given as $\mathbf{Q}$ and $\mathbf{R}$, respectively. $\mathbf{A}_d$, $\mathbf{B}_d$ and $\mathbf{C}_d$ are the system matrices of the discrete system, given in Equation (5.18).

An optimal state estimate, $\hat{\mathbf{x}}$, given these covariances can then be found for each time step using a Kalman filter with the following equations

$$\hat{\mathbf{x}}_k^- = \mathbf{A}_d\mathbf{x}_{k-1} + \mathbf{B}_d\mathbf{u}_{k-1} \tag{6.5}$$

$$\mathbf{P}_k^- = \mathbf{A}_d\mathbf{P}_{k-1}\mathbf{A}_d + \mathbf{Q} \tag{6.6}$$

$$\mathbf{K}_k = \mathbf{P}_k^-\mathbf{C}_d^T(\mathbf{C}_d\mathbf{P}_k^-\mathbf{C}_d^T + \mathbf{R})^{-1} \tag{6.7}$$

$$\hat{\mathbf{x}}_k = \hat{\mathbf{x}}_k^- + \mathbf{K}_k(\mathbf{y}_k - \mathbf{C}_d\hat{\mathbf{x}}_k^-) \tag{6.8}$$

$$\mathbf{P}_k = (\mathbf{I} - \mathbf{K}_k\mathbf{C}_d\mathbf{P}_k^-) \tag{6.9}$$

Each iteration of the Kalman filter first produces a prediction of the state, $\hat{\mathbf{x}}_k^-$, based on the estimate in the previous iteration (Equation 6.5). Then, in Equation 6.8, that prediction is updated with the measurement $\mathbf{y}_k$, giving the state estimate $\hat{\mathbf{x}}_k$. This state estimate can be used in the controller to provide feedback from the states.

Along with the estimates of the states, the Kalman gain $\mathbf{K}_k$ and the error covariance matrix $\mathbf{P}_k$ is also updated each iteration, in equations 6.6, 6.7 and 6.9. These equations, especially Equation 6.7 which contains a matrix inversion, is time-consuming to compute on a microcontroller without much processing power. However, these equations are independent of the measurements. Therefore, as long as the covariance matrices are constant, $\mathbf{K}_k$ may be computed offline [29]. The Kalman gain converges quickly, so only a few iterations of $\mathbf{K}_k$ need to be precomputed. The controller will then use these precomputed values of the $\mathbf{K}_k$ for the first few iterations, then use the steady-state value for all subsequent iterations.

An even simpler approach is to use the steady-state value of $\mathbf{K}_k$ for all iterations, including the first ones before it converges. The steady-state Kalman gain can be computed by iterating Equation 6.6, 6.7 and 6.9 enough times, or by solving the discrete algebraic Riccati equation, as explained in [15].

6.1.3   LQG Controller

An LQG controller was tested in simulations, and showed good performance (see Section 7.1). In the simulations, it was implemented as a continuous controller. This continuous controller is explained in more detail in [18]. When implemented on a microcontroller, it must be implemented as a discrete controller. The LQG controller is the combination of a Kalman filter and an LQR controller. The LQR controller is just a multiplication between

the states and the LQR gain matrix. This will not change in a discrete implementation, other than the fact that the discrete model must be used to compute the LQR gain. The continuous Kalman filter must be replaced by a discrete Kalman filter as described in Section 6.1.2.

Integral action is not included in an LQG controller. Some modifications must be made to the controller in order to include integral action, see [24] for a suggestion on how this is done.

6.1.4 Model Uncertainty

Several of the parameters are uncertain due to measurement difficulties and the fact that the system may change over time. Any model based controller will therefore most likely be based on a model which is incorrect. Model uncertainty reduces controller performance, but there are ways of handling uncertain models.

The simplest approach is using a non-model based controller, e.g. a PID controller. The performance of such a controller does not depend on knowledge of the model parameters. However, this controller requires accurate tuning instead. A poorly tuned PID controller may perform worse than a model based controller based on a slightly incorrect model.

Instead of deriving the model using equations describing the physical properties of the system and measuring the values of the parameters, the model could be found using system identification [19]. The model is found by applying experiments to the system, recording the input and output, and then using these to calculate a model.

Some of the parameters in the model seems to change over time. A model found by system identification or other means will therefore not be correct after the system has run for some time, even if it was correct at the time of identification. An adaptive controller could be used to determine the parameters of the system while running. It seems likely that this change over time is only due to the mechanical solutions of the prototype. It is therefore likely that in a final actuator, this will be much less of a problem. In this case, adaptive control should not be necessary.

6.2 Controller Implementation

As the controller runs on a microcontroller with a clock frequency of only 8 MHz, the computations must be fast in order to make the controller use a small sampling time. As mentioned in Section 6.1.2, the Kalman filter itself is a relatively complicated algorithm, but if the steady-state Kalman gain is

used, much of the computation can be done offline. The computations that have to be performed online during each iteration, are Equation (6.5) and (6.8), since they are the only equations dependent on the measurements.

The system is modeled using real numbers. Using real numbers with infinite precision is not possible on a computer, but floating point numbers give a fairly accurate approximation to this over a large range of values. Most microcontrollers, including the 8-bit Atmel microcontrollers used here, do not contain a floating point processor. Therefore floating point operations takes a long time to perform compared to integer operations. However, using integer operations for the computations is not possible for this controller. Some of the parameters in the model are very small, so the factor between the largest and smallest value in the system matrix is about 10^6. The alternative of fixed-point calculations would give inaccurate results, and is therefore not possible.

One optimization that may be performed is exploiting the fact that the system matrices contain a few zeros. The multiplications with the zero elements in the matrix do not need to be performed, since the result is of course zero. This optimization will be different for each matrix product, as the matrices have zeros at different places. Without this optimization, the same function can be used to perform all matrix products of the same size, no matter what matrices are involved. With this optimization, all matrix products will be performed in a different way from the other ones, so separate code must be written for each matrix product. Also, if at any time the model has to change, each matrix product needs to be rewritten in order to take into account new matrices with zeros at different places. For this reason, this optimization is not implemented.

Without any other optimizations than steady-state Kalman gain, the controller ran without any problems regarding execution time at a frequency of 120 Hz. As the gyro can only measure vibrations up to 140 Hz, increasing the controller frequency beyond this will not improve the performance of the controller.

6.2.1   Code

The controller was implemented as a program written in the C programming language, and was executed on the microcontroller on the circuit board.

The code is organized into different modules which are designed to be as independent as possible. The different modules and the interactions between them can be seen in Figure 6.3. In addition to these modules are modules for debug output and matrix operations which are used by several of the other modules.
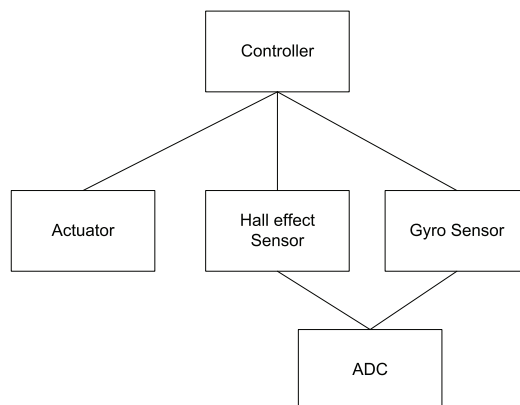
Figure 6.3: Code structure

Parts of the system are expected to change when the final system is created. A system modification means that the code also must be modified. With the code organized into independent modules, only the code related to the modified parts of the system, needs to be modified. As an example, the reference angle in this prototype is found by sampling the signal from the gyro. In the UAV, the camera system will not interact directly with the gyros, but with another microcontroller through a bus. In order to make this change, only the gyro module needs to be changed.

The main part of the code is the controller loop. Pseudocode of the controller loop can be seen in Listing 6.1.

Listing 6.1: Controller pseudocode

```
while(true) {
    Read sensor and gyro values
    Estimate system states using Kalman filter
    Calculate controller output
    Set the actuator value to the controller output
    Wait for next period
}
```

Chapter 7

Testing and results

7.1 Simulation

The system was originally simulated in [18], but due to the modeling error, some of the simulations have been rerun and their results presented here. The error was due to a division by the radius instead of a multiplication when converting from linear force to torque. This caused torque per current to be off by a factor of 10^4. In addition to fixing the error in the model, the parameters used in the simulation have been changed to the ones found in Section 5.4. No other changes have been made to the simulation, so the simulations do not, for example, contain the effect of the wires.

A PD controller with $K_p = 2$ and $K_d = 1$, gave a result as shown in Figure 7.1. The helicopter angle in the simulations was a random signal with a frequency distribution similar to the vibrations in the helicopter. From the figure, it can be seen that the low frequent vibrations are damped, but the bandwidth is low and vibrations from 10 Hz and up are not damped.

In order to compare the simulated results with the actual results (see Section 7.3), the system was also simulated using a 1 Hz sine wave as a reference. This result can be seen in Figure 7.2.

Using the controller parameters $K_p = 2$ and $K_d = 1$, the current peaks were about 4 A, which is significantly above the limit of 400 mA due to the motor driver. In order to make the current peaks go below 400 mA, both the proportional and derivative gain had to be reduced by a factor of $^1/_{10}$. However, this decreased performance significantly, as seen in Figure 7.3.

It was also possible to increase the controller gain quite significantly. Using controller parameters $K_p = 2 \cdot 10^3$ and $K_d = 1 \cdot 10^3$, the result is as shown in Figure 7.4. This result is almost as good as the results using the erroneous model in [18]. However, with these controller parameters, the peak
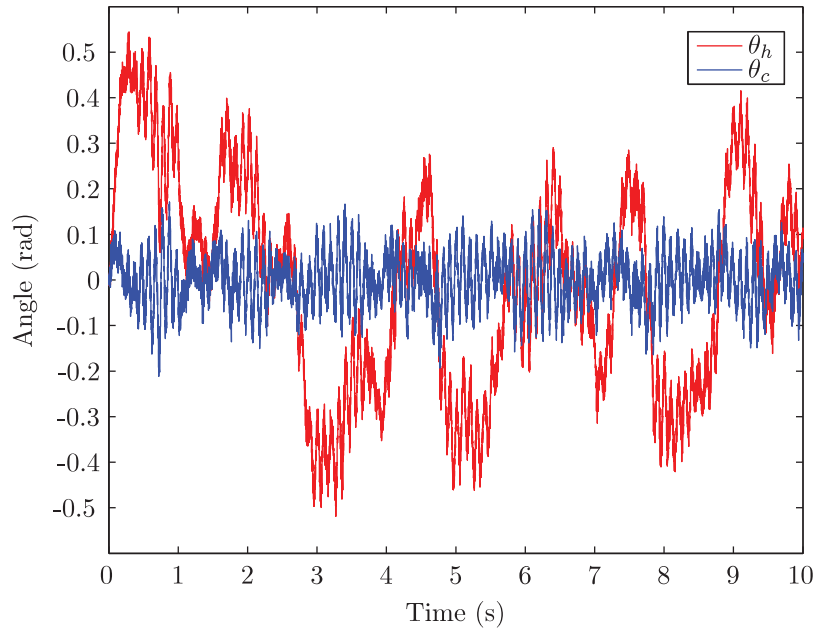
Figure 7.1: Simulated results using a PD controller under realistic frequency distribution of vibrations
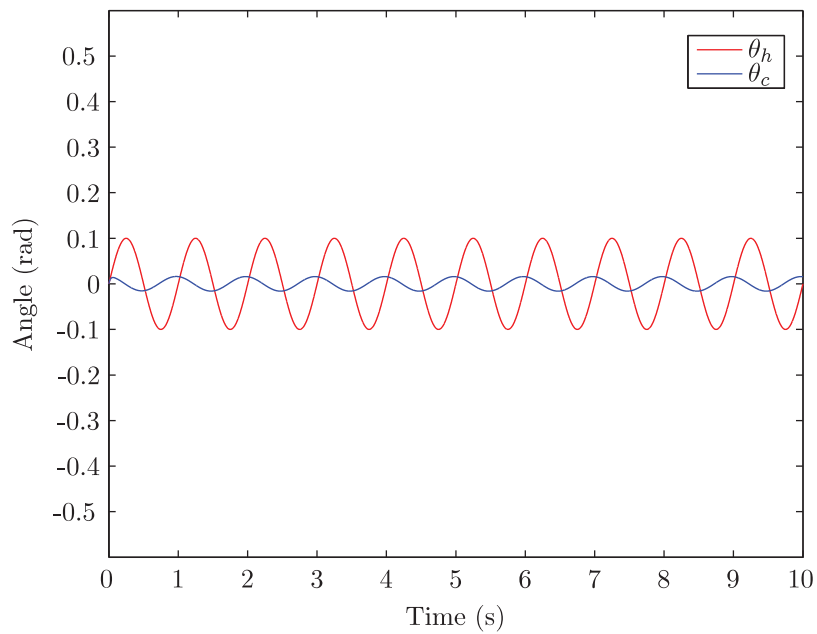

Figure 7.2: Simulated results using a PD controller with a 1 Hz sine wave as reference and controller parameters $K_p = 2$ and $K_d = 1$.
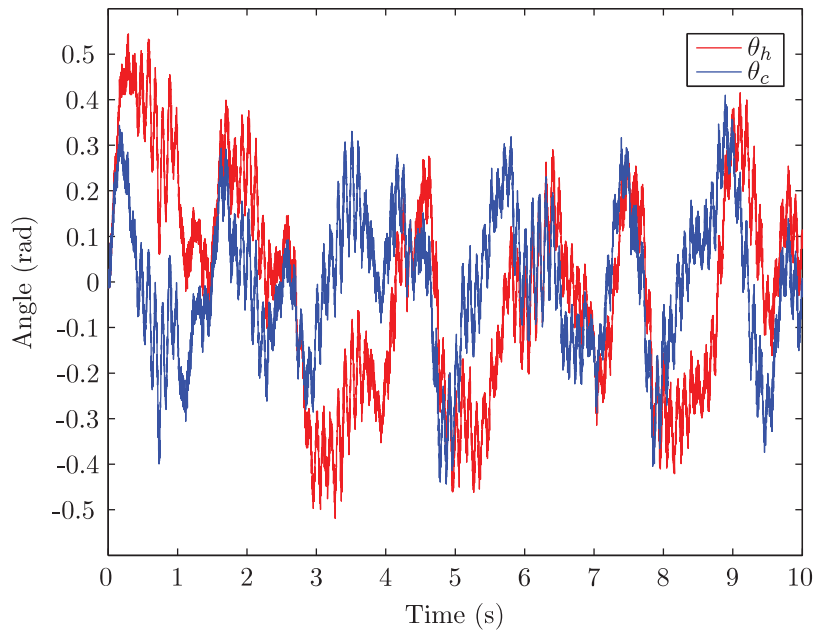
Figure 7.3: Simulated results using a PD controller with a 1 Hz sine wave as reference and controller parameters $K_p = 0.2$ and $K_d = 0.1$
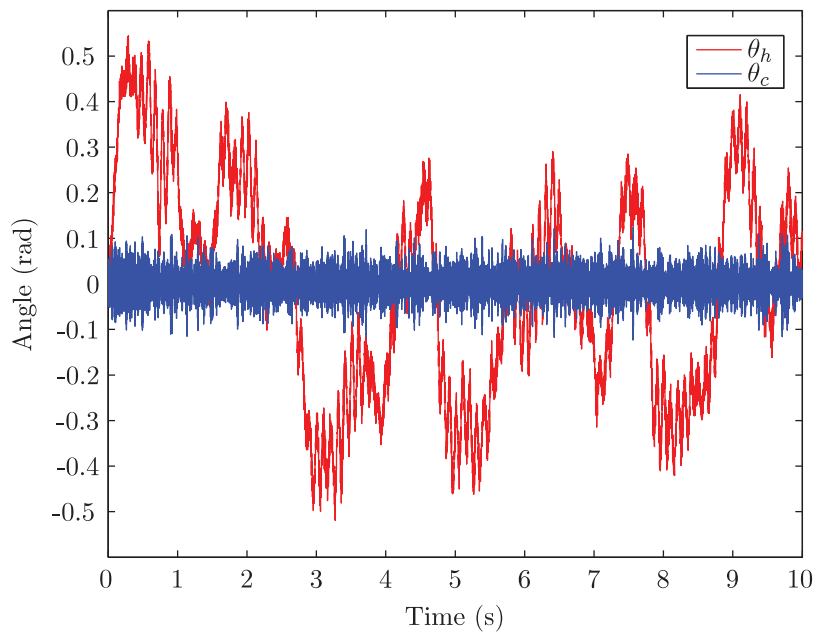

Figure 7.4: Simulated results using a PD controller with a 1 Hz sine wave as reference and controller parameters $K_p = 2 \cdot 10^3$ and $K_d = 1 \cdot 10^3$

49

currents were almost 5000 A, which is of course completely unrealistic.

The best results obtained in [18] was using an LQG controller. After fixing the model error, the result is as shown in Figure 7.5. The weight matrices used in the LQG controller was the same as the ones used in [18]:

$$\mathbf{Q} = \begin{bmatrix} 0 & 0 & 0 \\ 0 & 10^6 & 0 \\ 0 & 0 & 0 \end{bmatrix}$$

$$\mathbf{R} = 1$$

(7.1)

With these matrices, the result was slightly worse than the PD controller with $K_p = 2$ and $K_d = 1$. As the weight matrices determine the agressiveness of the controller, it would have been possible to increase the damping by tuning these matrices. This, however, causes increased current usage, just as it did for the PID controller.
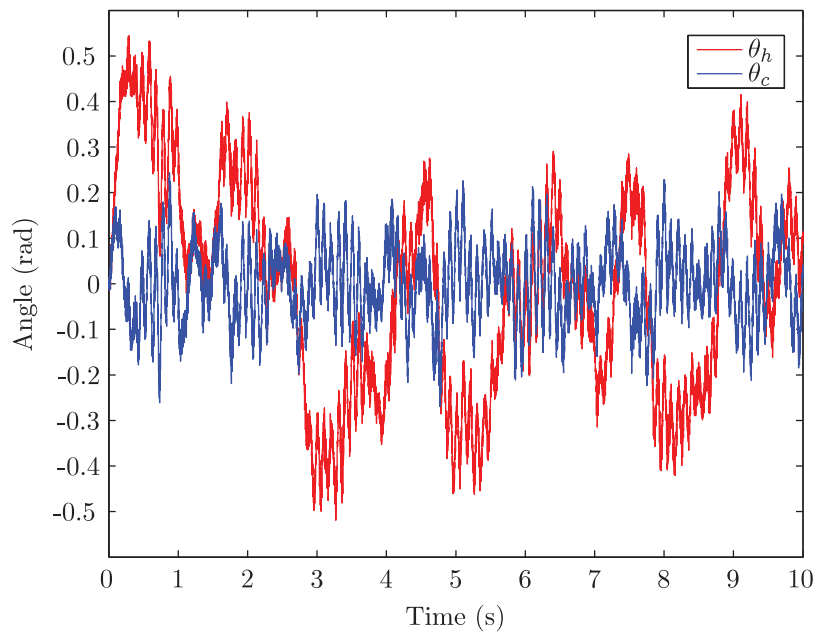
Figure 7.5: Simulated results using an LQG controller

7.2   Testing Procedure

The actuator was attached to the circuit board as shown in Figure 7.6, which means that the helicopter vibrations can be created by shaking the circuit

board. The moving part of the actuator should then, if the controller works, obtain an angle opposite of that of the circuit board.
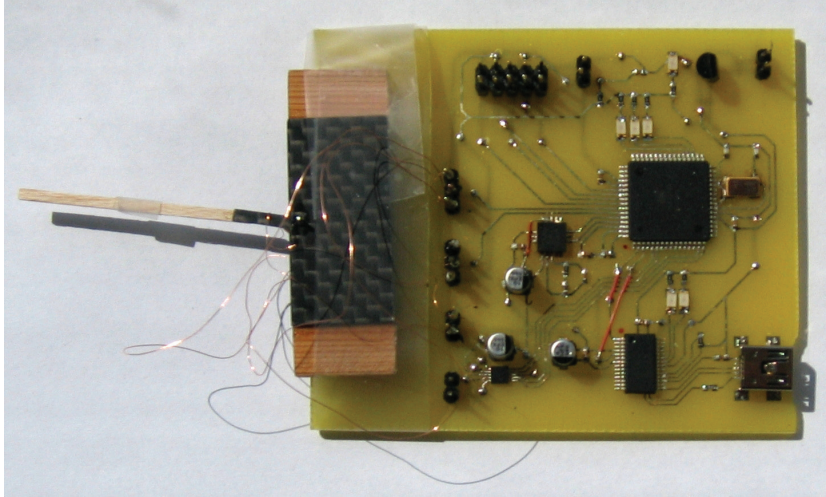
Figure 7.6: Actuator attached to circuit board

7.2.1 Helicopter Gyro

The reference to the controller is provided by a gyro mounted on the circuit board. This gyro is not completely free of noise. The datasheet [25] suggests adding a lowpass filter to the output in order to reduce the noise. However, this also reduces the bandwidth of the system, which is undesirable. The noise, however, is so small that it does not cause a problem.

A more serious issue is drifting. The gyro measures angular velocity. In order to use the measurements together with the angle measurements from the Hall effect sensors, the angular velocity from the gyros are integrated numerically in the code. In order to integrate the angular velocity, the zero level voltage (the output voltage when there is no movement) must be known. The integration is performed using the following equation:

$$\theta_{h,k} = \theta_{h,k-1} + \frac{(V_m - V_z)s}{F_s} \tag{7.2}$$

where V_m is the voltage measured this sample, V_z is the zero level voltage, s is the sensitivity, i.e. radians per volt and F_s is the sampling frequency. $\theta_{h,k}$ is the angle calculated during this iteration, while $\theta_{h,k-1}$ is the angle from last iteration.

If the value used for V_z is not exactly the zero level voltage, the angle computed by the integration will drift away from the actual value. Unfortunately, the zero level voltage is not constant. The zero-level voltage was measured to values between 1.213 V and 1.230 V. According to the datasheet [25], the zero-level voltage can change due to temperature, but only by 0.05°/s/°C. If the change in zero-level voltage observed here was only due to temperature, the temperature difference would be 102°C. There are clearly no temperatures this high in the system, so the difference must be caused by effects not specified in the datasheet or errors in the circuit board design. When the zero level voltage is not constant, it is not possible to find a correct value for V_z.

The gyro has a V_{ref} output which is meant to be the zero level at any time, regardless of the temperature or anything else. That means that V_{ref} can be subtracted from the output in order to get a signed number with zero level at 0. Unfortunately, this pin did not work. By measuring the voltage at the V_{ref} pin, and comparing it to the voltage at the output pins when there was no movement, it was seen that they were not the same. This pin could therefore not be used to fix the problem with gyro drift.

As long as the gyro drift is not too large, it is still possible to use the gyro as a reference to the controller. The ability of the controller to follow the reference from the gyro can still be obsserved, even though the reference angle is not exactly the angle of the circuit board. However, it can only run for a short time, until the gyro drifts outside of the limits of the actuator.

7.2.2 Camera Gyro

By studying the image from the camera while the circuit board is vibrating, it is possible to get qualitative results of the performance of the system. However, without heavy image analysis, it is not possible to use this image to get quantitative measurements of the system's ability to reduce the vibrations. In order to get quantitative measurements of the performance, a gyro can be used instead of the camera. This gyro measures the angle of the camera, θ_c, which can be compared to θ_h which is measured by the gyro on the circuit board.

The gyro at the end of the camera is the same as the gyro on the main circuit board. A small circuit board consisting of just the gyro and the required external components was created; a photo of it can be seen in Figure 7.7. The schematics and layout of this circuit board can be seen in Figure A.4 and A.5.

Unfortunately, it was not possible to use this gyro to measure the results. Just as the other gyro, this gyro also drifts, and the two gyros do not nec-
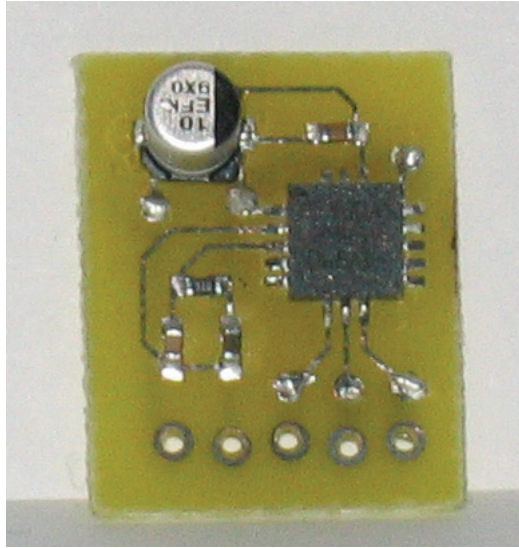
Figure 7.7: Circuit board with camera gyro

essarily drift in the same direction or by the same amount. Comparisons between these two gyros are therefore meaningless.

Also, the extra mass of this circuit board increases the moment of inertia, even when the circuit board is mounted as close as possible to the axis of rotation. This extra moment of inertia means that more current is required in order to accelerate the actuator. Because the current is limited to 400 mA, the extra moment of inertia means that the controller output goes into saturation more easily than without the extra gyro. This reduces the performance of the controller.

Due to these two problems, it was decided to use the Hall effect sensors instead of the extra gyro to measure the results.

7.3 Results from the Physical System

7.3.1 PI Controller

In the simulations, where wires were not included, steady state error was not a problem. However, for the physical system, a controller without integral action gave a significant steady state error. Unless the angles were extremely small, the performance was very poor. Therefore, integral action must be included in the controller.

Using a PI controller it was possible to get a result as shown in Figure 7.8. The controller is able to counter the low frequent change in reference, but at

higher frequencies additional noise is generated.
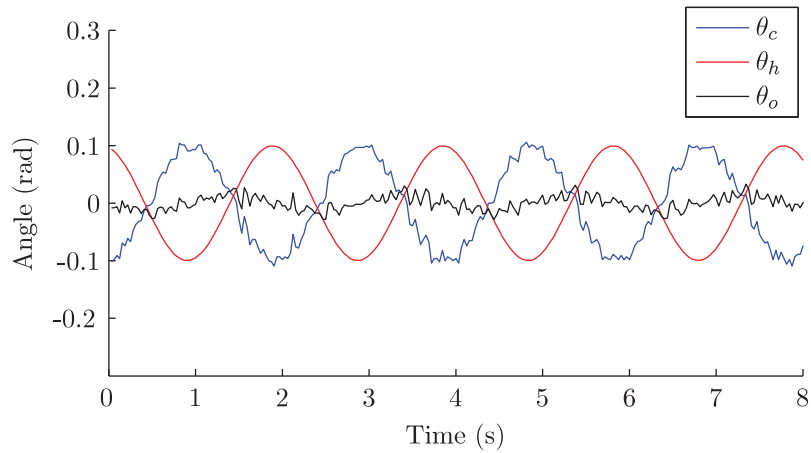
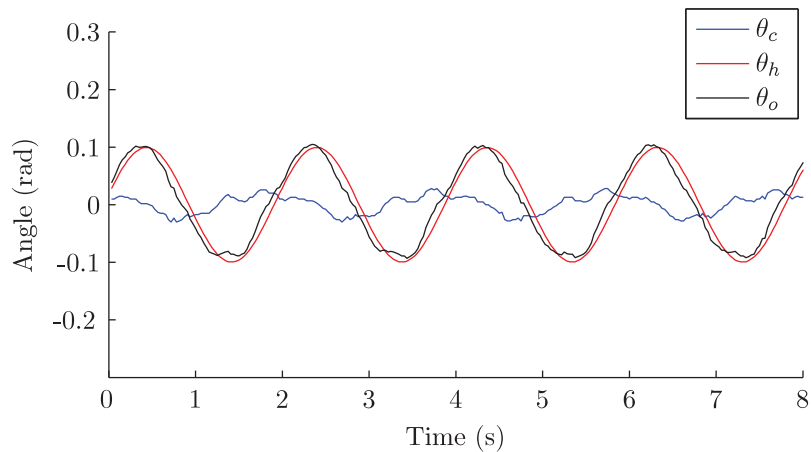Figure 7.8: Results with an artificial sine as reference

Figure 7.9: Results at a time where high gain could not be used

It was noted that the performance could change quite drastically over time without any changes to the controller parameters. The amount of gain possible without the system going unstable changed quite a lot. Figure 7.8 is the results from a time where a relatively high gain was possible ($K_p = 5$, $K_i = 500$). At other times, the system would go unstable at much lower gains. When the controller parameters were reduced to the point where the system was stable, the performance became very poor. For example, Figure 7.9 shows the results using controller parameters $K_p = 0.4$, $K_i = 25$.

Any higher gain made the system unstable. While the controller does counter the reference, it does so with significantly lower amplitude, so that the result is very poor. Both of these tests were done using a PI controller. Derivative action may increase the amount of gain possible while maintaining a stable system, and would most likely have increased the performance in both of these cases.

The main change in the system between the poor and good performance was the damping, due to friction and wires. An explanation to the results can be seen by looking at Bode plots of the system. Figure 7.10a, shows the Bode plot of the system with damping $d_w = 10^{-5}$. In order for the system to become stable, the magnitude of the transfer function must be lower than 0 for frequencies where the phase is less than $-180°$. Integral action is used in the controller, and integral action adds $-90°$ to the phase, which means that the magnitude must be less than 0 where the phase is less than $-90°$. One can then use a controller with a gain that increases the magnitude so that it is just below a necessary gain margin at $-90°$ phase. This gives a stable controller with a decent magnitude in the bandwidth area.

Compare this to Figure 7.10b where the damping is $^1/_{10}$ of the other figure. The magnitude of the transfer function has a resonance peak around $-90°$ phase. As this resonance top is closer to 0 dB than in the other bode plot, lower controller gain must be used. But when the magnitude of this peak is just below 0 dB, the magnitude at lower frequencies is even lower.

7.3.2 PID Controller and Kalman Filter

Including derivative action made it possible to increase the gain. A Kalman filter was used to calculate the derivative. Figure 7.11 compares the result with and without a Kalman filter. The controller is in both cases a PID controller with $K_p = 10$, $K_i = 200$ and $K_d = 1$. Derivative action was necessary in this case in order to use high gain without making the system unstable. Without a Kalman filter, the derivative was calculated using numerical differentiation, and as seen in Figure 7.11b, there is a lot of high frequent noise in the output. This is because differentiation amplifies noise. The Kalman filter gives an estimate of the states in the system without noise, and as seen in Figure 7.11a, this gives a much smoother result.

Figure 7.12 shows the result when the reference is a sine wave with different frequencies. The same controller was used in all cases, $K_p = 2$, $K_i = 200$, $K_d = 1$. In all cases, the controller follows the reference, but there is a small delay between the helicopter angle and the camera angle. For the low frequent vibrations in Figure 7.12a, this delay is not significant, so the result is good. However, with a higher frequency, this delay is significant, and at
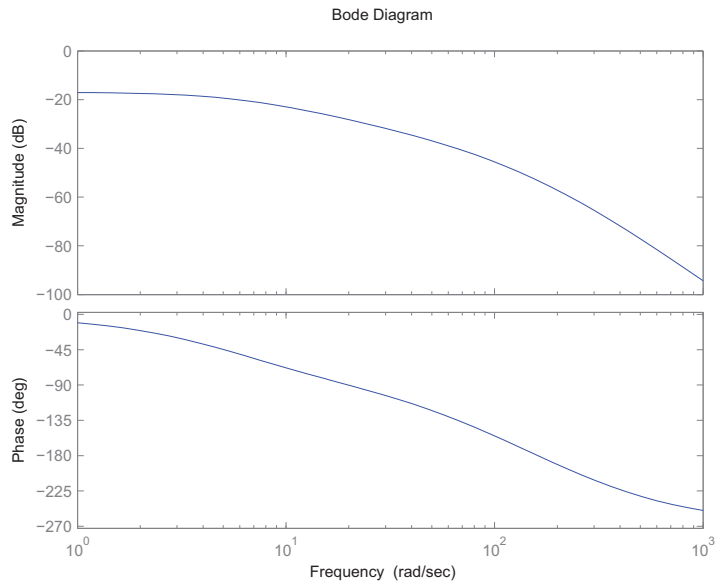
(a) $d_w = 10^{-5}$
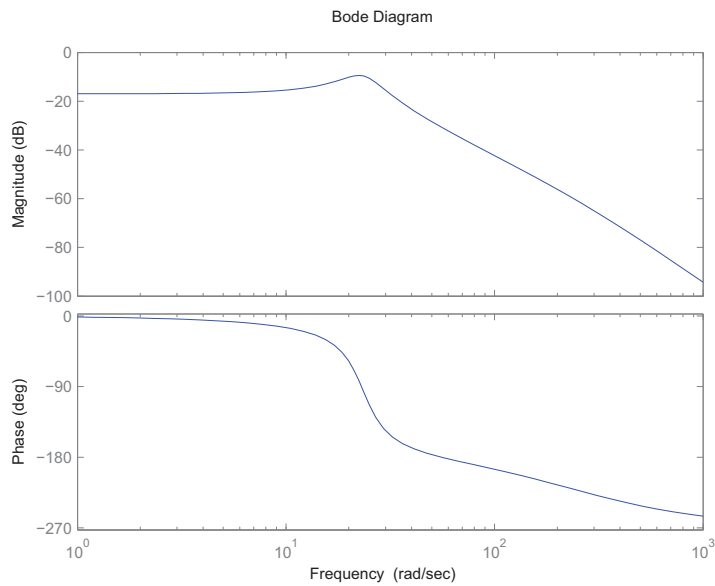
(b) $d_w = 10^{-6}$

Figure 7.10: Comparison of Bode plot for different damping values

5 Hz in Figure 7.12c, the delay makes the performance very poor.

Higher gain is necessary in order to reduce the delay. This is not possible,

though. As the current can at most be 400 mA, the controller output can be at most 1.5 V. Increasing the gain causes the controller output to saturate. Figure 7.13 shows the result and the controller output for a controller with controller parameters $K_p = 5$, $K_i = 200$, $K_d = 1$. The reference is a 2 Hz sine wave. The result can be compared to Figure 7.12b, where lower gain was used. It can be seen that saturation causes additional vibrations when the controller saturates. At even higher gains, where saturation becomes an even more significant issue, the system becomes unstable.
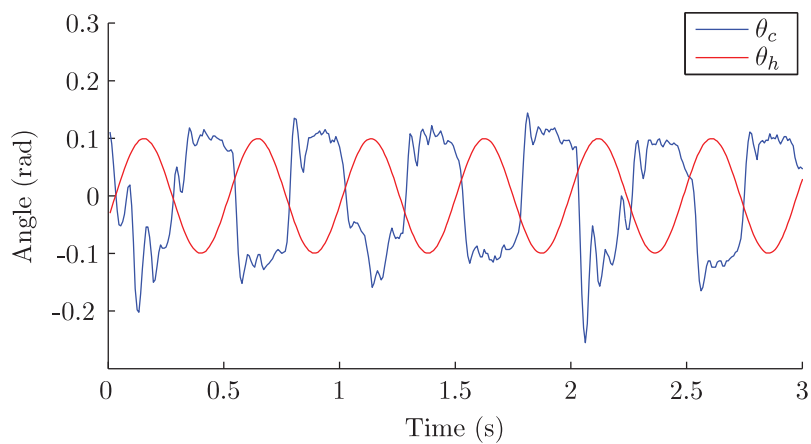
(a) With Kalman filter
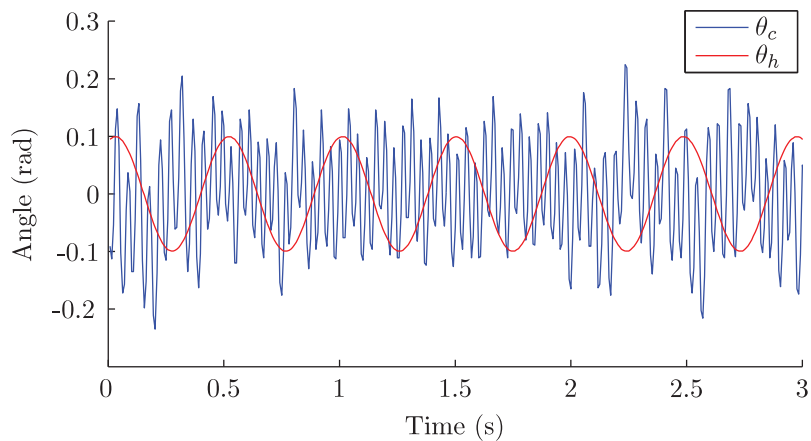
(b) Without Kalman filter

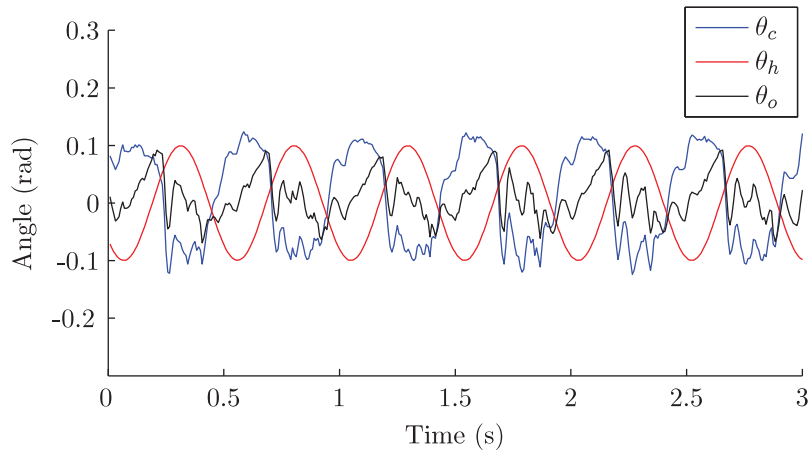Figure 7.11: Comparison of performance with and without Kalman filter
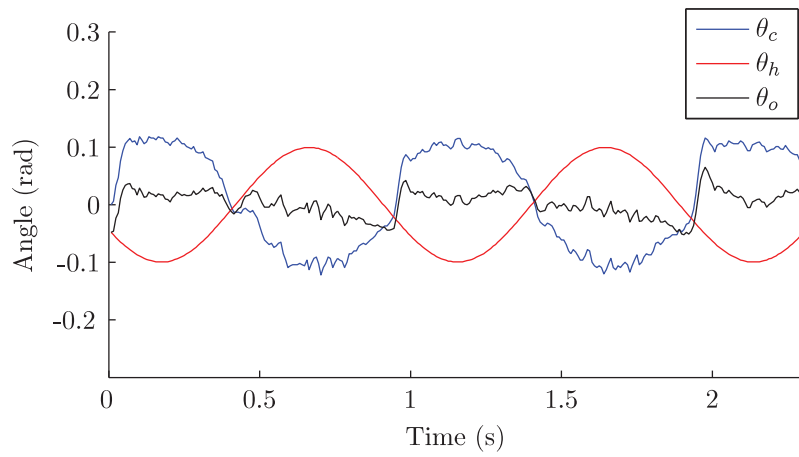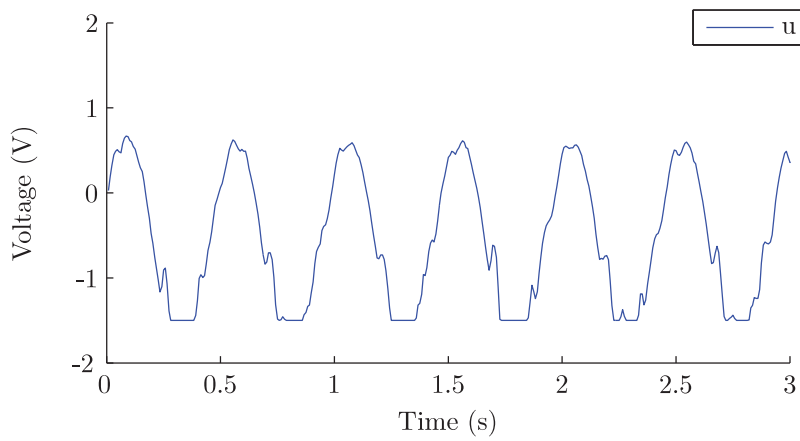
(a) 1 Hz
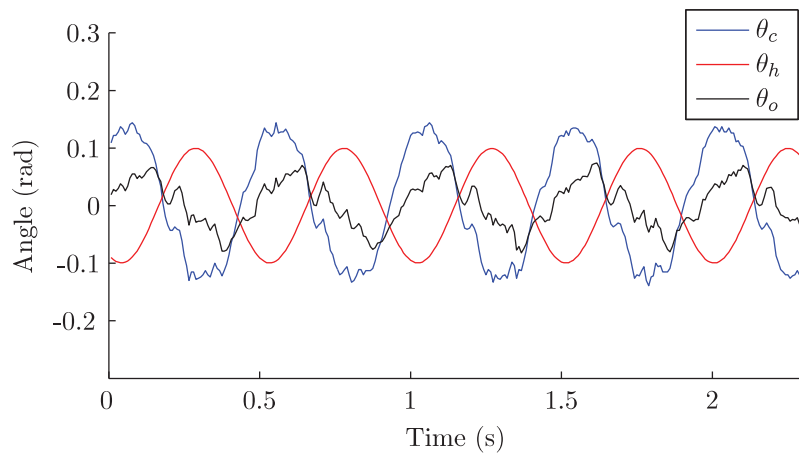
(b) 2 Hz
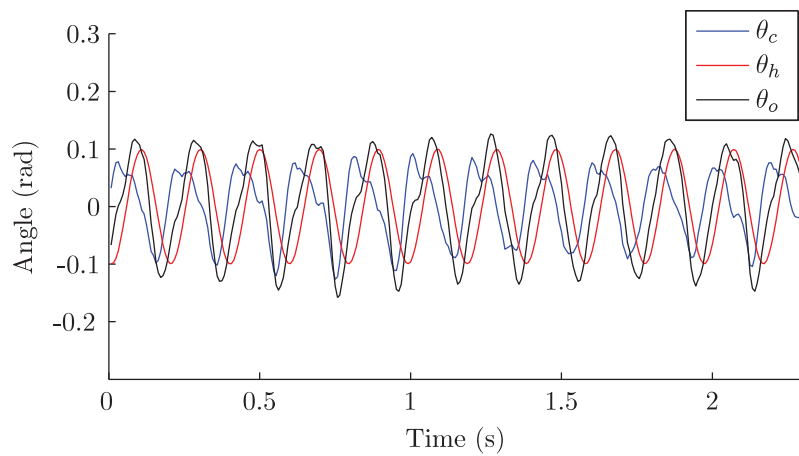
(c) 5 Hz

Figure 7.12: Comparison of results with different frequencies as reference

(a) Angles

(b) Controller output

Figure 7.13: Results with saturation

7.3.3 LQG Controller

The results using an LQG controller can be seen in Figure 7.14. The actuator does counter the reference, but the amplitude of θ_c is very small. This is expected because the LQG controller does not include integral action.
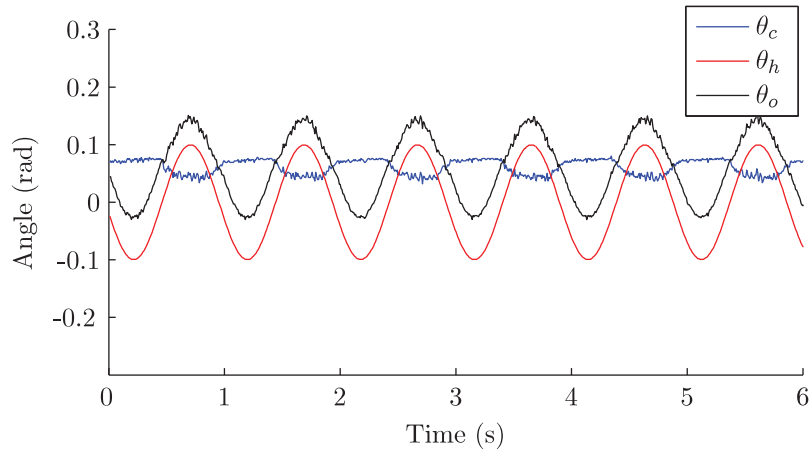

Figure 7.14: Results using an LQG controller

7.3.4 Reference from Gyro

The earlier tests were performed using an artificial reference instead of the angle from a gyro. It was difficult to test the system using measurements from the gyro. One reason for this is the gyro drift problem mentioned earlier. This made it difficult to ensure that the reference was within the limits that the controller could handle. Another issue was that when shaking the circuit board by hand, it was difficult to control the frequency of the vibrations; they would quite easily become higher than the bandwidth. A third issue was that moving the circuit board amplified the problems with the system parameters changing. Due to these issues, the performance of the controller was poor when shaking the circuit board, see Figure 7.15. However, some control is achieved, and it can be seen from the result that even though the result is relatively poor, the concept of stabilizing vibrations measured by a gyro works.
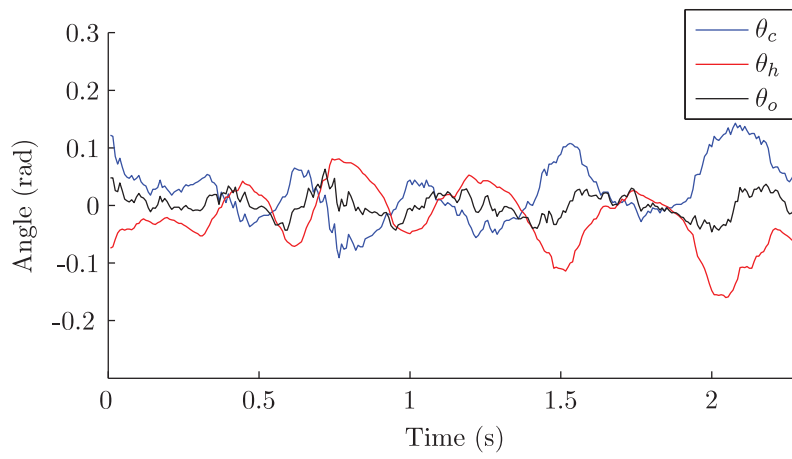
Figure 7.15: Results when shaking the circuit board by hand

Chapter 8

Discussion

8.1   Comments on the Results

The controller worked well at low frequencies, but had a relatively low bandwidth. The helicopter vibrations are concentrated around a few frequency bands, and only the low frequencies up to a few hertz were damped by the controller. The rotor frequency vibrations could be damped by passive stabilization. Since generating vibrations with frequencies this high is difficult, this could not be tested. The calculations show that these frequencies should receive damping, but testing is needed in order to confirm that this will work.

The 10 Hz frequencies were not possible to stabilize in this prototype by active control. Neither will they receive much damping from passive stabilization. Reducing the bandwidth of the passive stabilization in order to passively stabilize the 10 Hz vibrations will require extremely soft springs, and is most likely not possible. Increasing the bandwidth of the active control to more than 10 Hz should be possible, but will require more current. As the motor driver can only handle a current of 400 mA, another motor driver which can handle more current is required to prevent saturation.

The fact that the system changes over time contributes to the difficulty of controlling the system. It is likely that this problem will be much smaller in the final realization of the system, so it should not be necessary to use an adaptive controller which can take this into account. Even though the system will stay constant, it will still be difficult to model correctly, and there will certainly be model uncertainties in the final realization as well.

A Kalman filter is based upon a model of the system. Even though the model was not accurate, the Kalman filter worked well. It produced an estimate of the states which seemed close to reality, with far less noise than in the direct measurements. The controller worked far better with a Kalman

filter than without.

The PID controller is not based upon the model, so model uncertainties do not matter to the PID controller. However, the PID controller needs tuning. As the model changed during the tests, the controller had to be retuned quite often, and the tuning was most likely not ideal. Better results than obtained here could probably have been achieved with better tuning.

8.1.1 Comparisons between Simulated and Actual Results

The results from the simulations were similar to the results of the physical system. The performance was better when higher gain was used, but higher gain caused more current to be used.

The simulations were done using a PD controller, with similar actuator parameters as the physical system, but without integral action. Integral action was required in the physical system in order to overcome the steady-state error produced by the spring effect of the wires. As the system was simulated without the effect of the wires, it performed well, even without integral action.

When similar K_p and K_d, was used, the bandwidth and damping provided by the controller was similar in both the simulated and the physical system. However, there was a significant difference in current usage. In the physical system, the current was just on the limit of the motor driver, but in the simulations the current was almost 10 times as high. This is most likely caused by erroneous model parameters in the model used for simulation.

It was seen in the simulations that if current was not limited it was possible to increase the bandwidth significantly, at least to above 10 Hz. This indicates that the same is the case for the physical system; if higher currents were allowed, the bandwidth could increase.

Figure 7.2 and Figure 7.12a shows the simulations and actual system with a similar reference. Both give good damping of the low frequent variation in reference. However, in the physical system there are additional high frequent vibrations in the output, most likely due to measurement noise. This happens even though a Kalman filter is used in order to remove noise from the measurements. The simulations were performed without measurement noise, and the output is therefore without high frequent noise, even though a Kalman filter is not used.

8.2 Effect of Further Miniaturization

The prototype actuator has a mass of 3.66 g. In the final system, the mass needs to be reduced to about $^1/_{10}$ of this, in order to have two actuators plus camera and electronics weigh less than a gram.

The various parameters in the model scale differently with respect to the mass, so some effects will be more significant than they are in this prototype, while other will be less significant. The moment of inertia J of an object is typically proportional to mr^2. Since the radius scales with the mass, the moment of inertia will scale down faster than linearly. When J is reduced, less torque is required to produce the same angular acceleration.

The torque produced by an amount of current is given by $K_e r$. In order to reduce the power usage, it is an advantage to keep this factor as high as possible. K_e is dependent of the strength of the magnetic field B and the length of coil affected by the magnetic field. The length of coil affected by the magnetic field is again dependent on the number of coil turns and the size of the magnets. The mass of the coil wire is a very small part of the total mass, so it should not be necessary to reduce the number of coil turns. Smaller magnets may be necessary, and this may reduce both the area of wire affected by the magnetic field, and the field strength itself, depending on the shape and magnetic properties of the magnets. The radius will of course scale down with the rest of the actuator. It is possible to reduce the air gap around the coil in order to increase the magnetic field and thus increasing K_e. However, the air gap is already small, so the effect of this is limited. In sum, $K_e r$ will scale down, with the mass, but most likely not as fast as the moment of inertia. Less current will be required in order to accelerate the actuator.

The spring/damper effect of the wires is almost completely independent of the size of the actuator. If the spring constant does not scale down with the rest of the actuator, but $K_e r$ does, higher current is required in order to overcome the torque from the spring constant. Since the moment of inertia scales down, more of the torque must be used to overcome the torque from the wires compared to what is required to accelerate the actuator. Also, the prototype actuator was only tested for small angles, far smaller than desired in an actual setting. At larger angles, the wires will produce an even larger torque due to the spring effect.

When the moment of inertia is reduced, the effect of passive stabilization is also reduced, i.e. it will only work for higher frequencies than it did in this prototype. To prevent this, the spring constant must also be reduced.

Due to these issues, the spring constant from the wires should be reduced by a similar amount as the moment of inertia. If that is possible, the passive

damping will stay the same, and the current required to overcome the spring will not increase. If this cannot be done, camera stabilization will be more difficult, with worse performance of both active and passive damping.

Chapter 9

Conclusion

In this thesis, a prototype of a camera stabilization system for a nano-UAV has been constructed. The camera stabilization system uses voice coil actuators to move the camera and Hall effect sensors to measure the position. An actuator was built, and a circuit board for controlling the camera was created. A controller for the system was implemented on a microcontroller.

Testing showed that the idea of stabilizing a camera using a voice coil actuator and Hall effect sensor worked well in principle. Unfortunately, the bandwidth of the controller was lower than desired. Saturation of the current due to limitations in the motor driver prevented higher gain from being used which seems to be the main reason for the low bandwidth. It is believed that if higher currents were allowed, higher bandwidth could be achieved. High frequencies will be damped by passive stabilization, due to the wires between the actuator and the circuit board. Unfortunately, frequencies around 10 Hz are not significantly damped by either active or passive stabilization.

9.1 Further Work

In order to be used on a nano-UAV, the entire camera stabilization system must have a mass of less than 1 g. The prototype created in this thesis is about 10 times too large, so in order to use this system for its intended purpose, the system must be miniaturized. Miniaturization introduces some new challenges which need to be sorted out, both in the mechanical design and in controller design.

Only one axis was implemented in this prototype. The original intent was to stabilize the camera around both the pan and tilt axes, so the system must be extended to two axes.

The bandwidth of the controller was not as high as desired. It was high

enough to stabilize the low-frequent disturbances up to 1 Hz, and passive damping from the wires will provide stabilization of the rotor frequencies at multiples of 85 Hz. However, the vibrations around 10 Hz was not handled by either the active or the passive stabilization. This problem must be solved, and the best approach will most likely be to improve the controller in order to increase the bandwidth to more than 10 Hz.

Bibliography

[1] Allegro Microsystems. A1395 datasheet. `http://www.allegromicro.com/en/Products/Part_Numbers/1391/1391.pdf`.

[2] Allegro Microsystems. A1395 materials declaration report. `http://www.allegromicro.com/en/Products/Composition/index.asp?PN=A1395SEHLT-T`.

[3] Allegro Microsystems. A3901 datasheet. `http://www.allegromicro.com/en/Products/Part_Numbers/3901/3901.pdf`.

[4] Allegro Microsystems. A3901 materials declaration report. `http://www.allegromicro.com/en/Products/Composition/index.asp?PN=A3901SEJTR-T`.

[5] Asahi Kasei. HG-0111 datasheet. `http://www.asahi-kasei.co.jp/ake/en/product/hall/file/hg-0111_e.pdf`.

[6] Atmel. 32-Pad MLF package material declaration. `http://atmel.com/green/documents/pmdds/MLF_32_Sn.pdf`.

[7] Atmel. ATMega128A datasheet. `http://atmel.com/dyn/resources/prod_documents/doc8151.pdf`.

[8] J. G. Balchen, T. Andresen, and B. A. Foss. *Reguleringsteknikk*. Institutt for teknisk kybernetikk, 2003.

[9] R.G. Brown and P.Y.C. Hwang. *Introduction to random signals and applied Kalman filtering*. John Wiley & Sons, third edition, 1997.

[10] J. Catsoulis. *Designing embedded hardware*. O'Reilly Media, Inc., 2005.

[11] Wyatt Emery Davenport. Development, modeling and simulation of a nano aerial vehicle using empirical data. Master's thesis, University of Missouri–Rolla, 2007.

[12] W.A. Davis. Nano air vehicles - a technology forecast. Air War College, Center for Strategy and Technology, 2007.

[13] C.W. de Silva. *Vibration and shock handbook*. CRC Press, Taylor & Francis Group, 2005.

[14] Future Technologies. FT232R datasheet. `http://atmel.com/dyn/resources/prod_documents/doc8151.pdf`.

[15] M.S. Grewal and A.P. Andrews. *Kalman filtering: theory and practice using MATLAB*. John Wiley & Sons, second edition, 2001.

[16] H2W Technologies. Limited angle torque motors. `http://www.h2wtech.com/pdfs/Limited%20Angle%20Torque%20Motor.pdf`.

[17] Honeywell. Hall effect sensing and applications. `http://content.honeywell.com/sensing/prodinfo/solidstate/technical/hallbook.pdf`.

[18] Sindre Kjenstad. One-gram stabilized pan/tilt microcamera. NTNU, 2009.

[19] Lennart Ljung. *System identification: theory for the user*. Prentice Hall, second edition, 1999.

[20] Michael J. Logan, Julio Chu, Mark A. Motter, Dennis L. Carter, Michael Ol, and Cale Zeune. Small uav research and evolution in long endurance electric powered vehicles. *American Institute of Aeronautics and Astronautics*, 2007.

[21] Prox Dynamics. Micro helicopters and ornithopters, 2009. `http://www.proxdynamics.com/r_d/micro_helicopters_and_ornithopters/`.

[22] Prox Dynamics. PD-100 Black Hornet information folder, 2009. `http://www.proxdynamics.com/images/uploads/Black-Hornet-June-2009.pdf`.

[23] D. Sachs, S. Nasiri, and D. Goehl. Image stabilization technology overview. `http://www.invensense.com/cn/shared/pdf/ImageStabilizationWhitepaper_051606.pdf`.

[24] S. Skogestad and I. Postlethwaite. *Multivariable feedback control: analysis and design*. John Wiley & Sons, second edition, 2007.

[25] STMicroelectronics. LPY530AL datasheet. `http://www.st.com/stonline/products/literature/ds/15807/lpy530al.pdf`.

[26] STMicroelectronics. Mems gyroscopes. `http://www.st.com/stonline/domains/support/epresentations/memsgyroscopes/gyros.htm`.

[27] P.A. Tipler and G. Mosca. *Physics for Scientists and Engineer*. WH Freeman, 2004.

[28] G. Warwick. DARPA sets nano-UAV challenge. *Flight International*, 168(5005):24, 2005.

[29] G. Welch and G. Bishop. An introduction to the Kalman filter. Technical Report TR 95-041, University of North Carolina at Chapel Hill, 2006.

Appendix A

Circuit board schematics
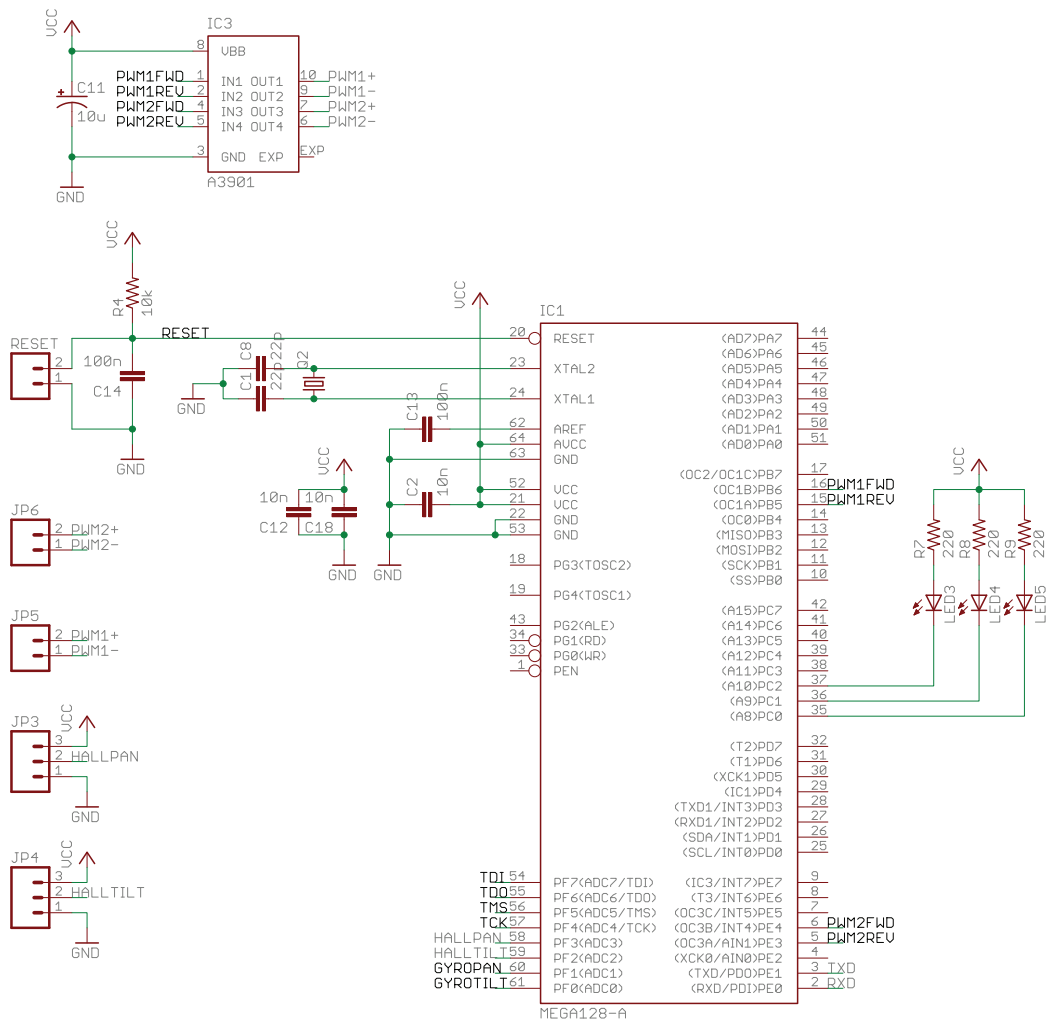
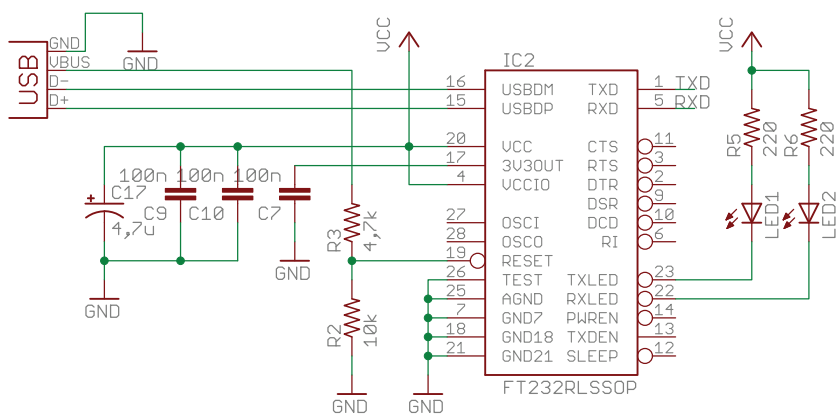Figure A.1: Schematic of circuit board (page 1)
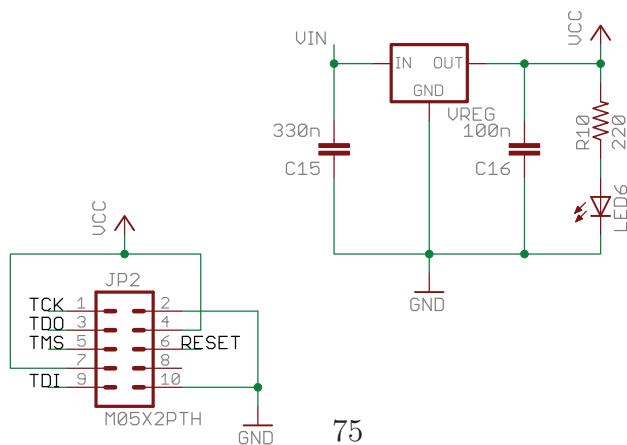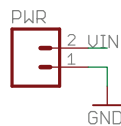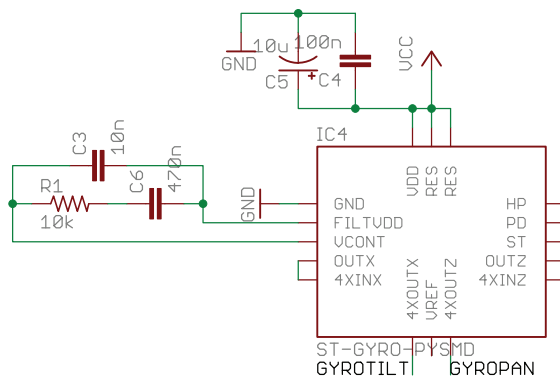
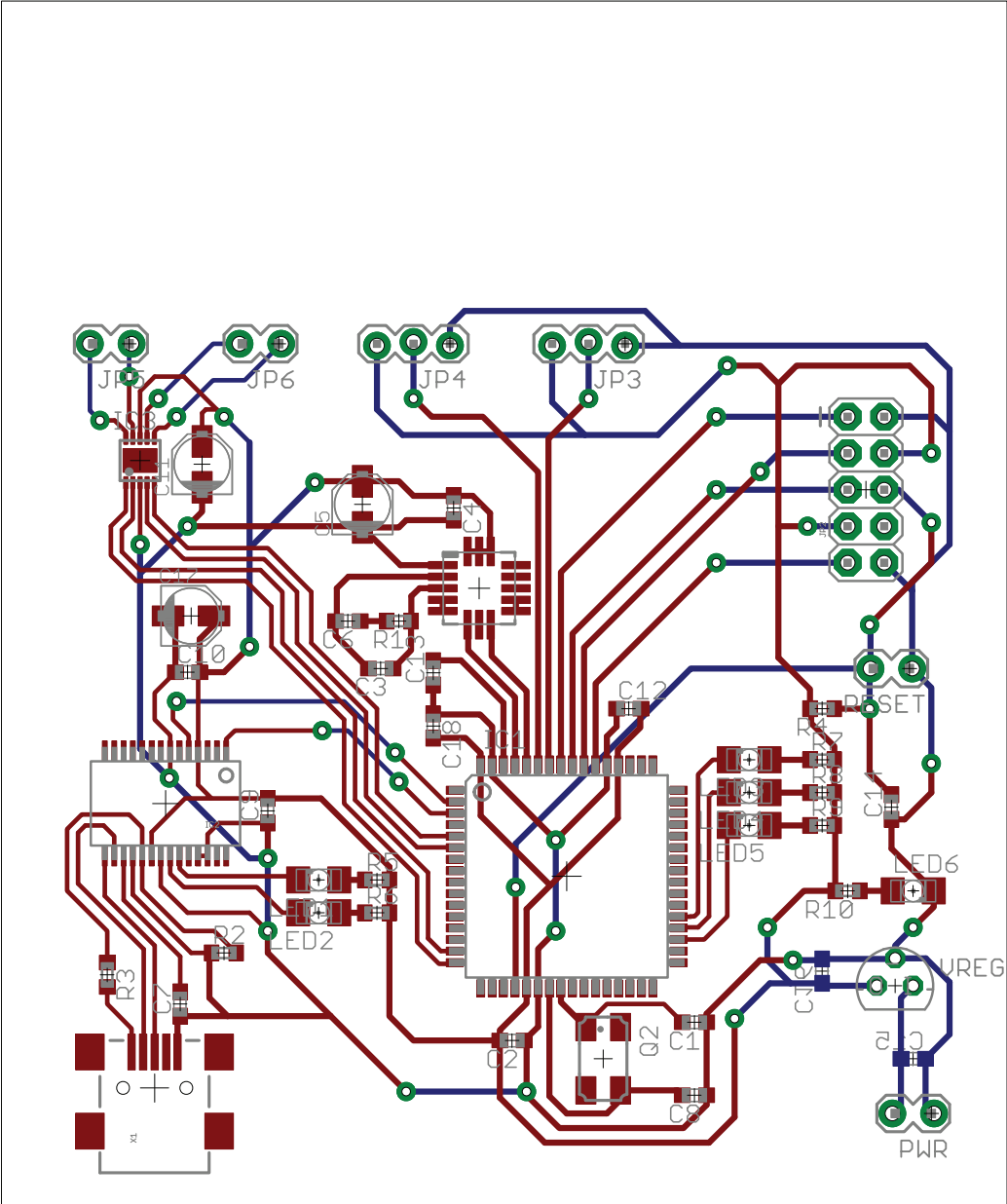Figure A.2: Schematic of circuit board (page 2)
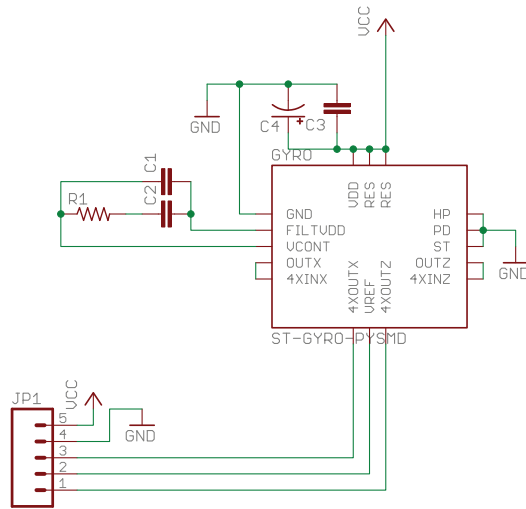
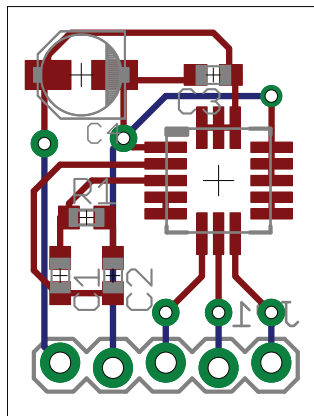Figure A.3: Circuit board layout

Figure A.4: Schematic of circuit board for the camera gyro

Figure A.5: Layout of circuit board for the camera gyro